

Modelling of Lewis Number dependence of Scalar dissipation rate transport for Large Eddy Simulations of turbulent premixed combustion

Yuan Gao^{a)}, Nilanjan Chakraborty^{a)}*

^{a)} School of Mechanical and Systems Engineering, Newcastle University, Claremont Road, Newcastle-Upon-Tyne, NE1 7RU, UK

*Corresponding author.

Email: nilanjan.chakraborty@ncl.ac.uk

Phone No: +44 0191 208 3570

Fax No: +44 0191 208 8600

* Corresponding author

ABSTRACT

The influences of differential diffusion of heat and mass on the Favre-filtered scalar dissipation rate (SDR) transport have been analysed and modelled using *a-priori* analysis of Direct Numerical Simulations (DNS) data of freely propagating statistically planar turbulent premixed flames with different values of global Lewis number Le . The DNS data has been explicitly filtered using a Gaussian filter to obtain the unclosed terms of the Favre-filtered SDR transport equation, arising from turbulent transport (T_1), density variation due to heat release (T_2), strain rate contribution due to the alignment of scalar and velocity gradients (T_3), correlation between the gradients of reaction rate and reaction progress variable (T_4), molecular dissipation of SDR ($-D_2$) and diffusivity gradients $f(D)$. The statistical behaviours of these terms and their scaling estimates reported in a recent analysis have been utilised here to propose models for these unclosed terms in the context of Large Eddy Simulations (LES) and the performances of these models have been assessed using the values obtained from explicitly filtered DNS data. These newly proposed models are found to satisfactorily predict both the qualitative and quantitative behaviours of these unclosed terms for a range of filter widths Δ for all Le cases considered here.

Keywords Scalar Dissipation Rate, Large Eddy Simulations, Direct Numerical Simulation, *a-priori* analysis, turbulent premixed combustion, Lewis number

NOMENCLATURE

Arabic

c	Reaction progress variable
c_m	Thermo-chemical parameter
C_p	Specific heat at constant pressure
C_v	Specific heat at constant volume
C_F	Model parameter
C_3, C_4	Model parameters
D	Progress variable diffusivity
D_t	Eddy diffusivity
Da	Damköhler number
D_1	Molecular diffusion term
D_2	Molecular dissipation term
f_b	Burning mode probability density function
f_{T_2}, f_{T_3}, f_{TD}	Model parameters
$f(D)$	Term due to diffusivity gradient
k_{sgs}	Sub-grid scale kinetic energy
K_c^*	Thermo-chemical parameter
Ka	Karlovitz number
Le	Lewis number
l	Integral length scale
Ma	Mach number
M_i	i^{th} component of resolved flame normal
N_c	Scalar dissipation rate
N_i	i^{th} component of flame normal
p	Model parameter
Pr	Prandtl number
Q	General quantity
Re_t	Turbulent Reynolds number
Re_Δ	Sub-grid Reynolds number
S_L	Unstrained laminar burning velocity
t	Time
t_c	Chemical time scale
t_f	Initial turbulent eddy turnover time
t_{sim}	Simulation time
T	Temperature
T_{ad}	Adiabatic flame temperature
T_0	Reactant temperature
T_1, T_2, T_3, T_4	Terms in the transport equation of Favre filtered scalar dissipation rate
u_i	i^{th} component of non-dimensional fluid velocity
u'	Root mean square fluctuation of velocity
u'_Δ	Sub-grid velocity fluctuation

\dot{w}	Chemical reaction rate
x_i	i^{th} Cartesian co-ordinate
Y_R	Reactant mass fraction
Y_{R0}	Reactant mass fraction in unburned gas
$Y_{R\infty}$	Reactant mass fraction in burned gas

Greek

α_T	Thermal diffusivity
α_{T0}	Thermal diffusivity of the unburned gas
β	Zel'dovich number
β_3, β'_3	Model parameters
γ	Ratio of specific heats ($= C_p / C_v$)
γ_1, γ_2	Model parameter
δ_{th}	Thermal flame thickness
δ_z	Zel'dovich flame thickness
Δ	Filter width
Γ	Model parameter
μ	Viscosity
μ_0	Viscosity of unburned gas
ρ	Density
ρ_0	Unburned gas density
τ	Heat release parameter
τ_{ij}	Viscous stress tensor
Φ'	Model parameter

Symbol

\bar{q}	LES filtered value of a general quantity q
\tilde{q}	Favre filtered value of a general quantity q

Subscript

0	Unburned gas value
∞	Burned gas value
<i>res</i>	Resolved scale value
<i>sg</i>	Sub-grid scale value

Acronyms

DNS	Direct Numerical Simulation
LES	Large Eddy Simulation
PDF	Probability density function
SDR	Scalar Dissipation Rate

1. INTRODUCTION

Lean premixed combustion has been identified as one of the possible ways to reduce pollutant emission from gasoline engines and industrial gas turbines [1]. Lean hydrogen and hydrogen-blended hydrocarbon combustion have the potential to attenuate pollutants and greenhouse gas emissions [2,3]. However, the flames with abundance of fast diffusing species such as hydrogen either in molecular or in atomic form give rise to significant level of differential diffusion of heat and mass. The differential diffusion of heat and mass can be characterised by a non-dimensional number known as the Lewis number Le , which is defined as the ratio of thermal diffusivity α_T to mass diffusivity D (i.e. $Le = \alpha_T / D$). In actual premixed combustion it is often not straightforward to assign a single global Lewis number in the presence of several species with different Lewis numbers. Often the Lewis number of the deficient species is considered to be the global Lewis number [4], whereas Law and Kwon [5] proposed a methodology of evaluating the effective Lewis number based on heat release measurements. More recently Dinkelacker *et al.* [6] proposed an algebraic expression for the effective Lewis number based on mole fractions of major species. A number of previous analyses concentrated on the effects global Lewis number on different aspects of premixed combustion in isolation [7-28] and the same approach has been adopted here.

Modelling of the differential diffusion arising from non-unity global Lewis number remains pivotal to high-fidelity engineering simulations, which are likely to play important roles in the development of new generation combustors using either hydrogen or hydrogen-blended fuels. Prediction of micro-mixing rate of hot products and cold unburned gas plays a key role in the modelling of turbulent reacting flows and a quantity known as the scalar dissipation rate (SDR) characterises this micro-mixing rate [29,30-32]. Furthermore, the Favre-mean value of SDR of reaction progress variable c in premixed turbulent flames can be related to the mean reaction rate in the context of Reynolds Averaged Navier Stokes (RANS) simulations [23,33-35]. The instantaneous SDR of reaction progress variable is defined as [23,33-38]:

$$N_c = D \nabla c \cdot \nabla c \quad (1)$$

where D is the diffusivity of reaction progress variable c . Recent analyses have demonstrated [36-38] that the SDR based reaction rate closure for RANS can also be used for the modelling of the filtered reaction rate $\overline{\dot{w}}$ based on the Favre-filtered SDR of reaction progress variable (i.e. $\tilde{N}_c = \overline{\rho D \nabla c \cdot \nabla c} / \bar{\rho}$) in the context of Large Eddy Simulation (LES) in the following manner when the filter size Δ remains greater than the thermal flame thickness $\delta_{th} = (T_{ad} - T_0) / \text{Max}|\nabla T|_L$ (where T_{ad}, T_0 and T are the adiabatic flame, unburned gas and instantaneous temperatures respectively):

$$\bar{w} = \frac{2\bar{\rho}\tilde{N}_c}{(2c_m - 1)} \quad \text{with} \quad c_m = \frac{\int_0^1 [c\dot{w}]_L f_b(c) dc}{\int_0^1 [\dot{w}]_L f_b(c) dc} \quad (2)$$

where ρ is the density and $\tilde{Q} = \overline{\rho Q} / \bar{\rho}$ is the Favre-filtered value of a quantity Q with the over-bar indicating an LES filtering operation. In eq. 2 $f_b(c)$ is the reacting mode probability density function (pdf) of c and the subscript ‘L’ refers to the planar laminar flame conditions. By assuming $f_b(c)$ as a smooth function, regardless the exact form, the numerical value of c_m remains within a range of 0.7-0.9 for typical hydrocarbon-air mixtures [33].

The modelling of SDR is not only useful for the closure of filtered reaction rate but it also plays a pivotal role in the closure of micro-mixing rate in the context of pdf methodology [30,39-41]. For turbulent premixed flames, the Favre-filtered SDR \tilde{N}_c can be modelled either by using an algebraic expression in terms of the resolved quantities or by solving a modelled transport equation. A few recent analyses [36-41] have concentrated on the algebraic closure of SDR for turbulent premixed flames in the context of LES. Algebraic closures are suitable when an equilibrium is maintained between the generation and destruction rates of \tilde{N}_c but this assumption may be rendered invalid under some conditions (e.g. low Damköhler number lean premixed combustion). A number of previous analyses [34, 42-51] concentrated on the modelling of SDR transport in turbulent premixed combustion in the context of RANS simulations. Interested readers are referred to Ref. [34] for a detailed review of the existing modelling methodologies for SDR transport in the context of RANS simulations. Recent advancements in high performance computing have made LES of industrial flows more affordable than in the past, and LES is more successful in capturing unsteady flow features than RANS. However, relatively limited attention has been given to the investigation of SDR transport in the context of LES [52,53]. Recently, models for the unclosed terms of the SDR \tilde{N}_c transport equation for unity Lewis number flames in the context of LES have been proposed [53] but the differential diffusion effects due to non-unity Le were not addressed. A recent analysis [28] concentrated on the influences of global Le on the statistical behaviours of the unclosed terms of the \tilde{N}_c transport equation based on an order-of-magnitude approach, which successfully explained the effects of global Le and the filter width Δ dependences of the Favre-filtered SDR \tilde{N}_c and its transport. It has been found that Le has significant influences on both the qualitative and quantitative behaviours of the unclosed terms of the SDR \tilde{N}_c transport equation [22, 28] but the modelling of Le

effects on these unclosed terms is yet to be addressed, and the present analysis aims to address this gap in the existing literature. In this respect the main objectives of this paper are:

- (i) To propose models for the unclosed terms of the SDR transport equation in such a manner that the performances of these models remain satisfactory for a range of Δ and Le .
- (ii) To assess the performances of the newly proposed models with respect to explicitly filtered Direct Numerical Simulation (DNS) data.

These objectives are addressed here by conducting *a-priori* analysis using a DNS database of statistically planar turbulent premixed flames with a range of different values of Le (i.e. $Le = 0.34-1.2$). The details related to mathematical background and numerical implementation are provided in the next section. This is followed by the presentation of the results and subsequent discussion. The main findings are summarised and conclusions are drawn in the final section of this paper.

2. MATHEMATICAL BACKGROUND & NUMERICAL IMPLEMENTATION

Three-dimensional DNS simulations with detailed chemistry are now possible but they remain extremely expensive and need several millions of CPU hours [54] for conducting extensive parametric variations and carrying out explicit filtering of DNS data using a range of filter widths Δ , as has been done in the current study. Thus, the chemical mechanism has been simplified here as a single-step Arrhenius type irreversible chemical reaction. Under this condition the species field is uniquely represented by a reaction progress variable c , which can be defined by using the mass fraction of a suitable reactant Y_R as: $c = (Y_{R0} - Y_R)/(Y_{R0} - Y_{R\infty})$, where subscripts 0 and ∞ denote the values in the unburned and burned gases respectively. The transport equation of c can be used to derive a transport equation of $\tilde{N}_c = \overline{\rho D \nabla c \cdot \nabla c} / \bar{\rho}$, which takes the following form [28,53]:

$$\frac{\partial(\bar{\rho}\tilde{N}_c)}{\partial t} + \frac{\partial(\bar{\rho}\tilde{u}_i\tilde{N}_c)}{\partial x_i} = \underbrace{\frac{\partial}{\partial x_i} \left(\rho D \frac{\partial N_c}{\partial x_i} \right)}_{D_1} + T_1 + T_2 + T_3 + T_4 - D_2 + f(D) \quad (3)$$

where u_i is the i^{th} component of velocity vector. On the left hand side of eq. 3 the terms denote the transient effects and resolved advection of \tilde{N}_c respectively. The term D_1 depicts the molecular diffusion of \tilde{N}_c , and the terms $T_1, T_2, T_3, T_4, (-D_2)$ and $f(D)$ are all unclosed and expressed as:

$$T_1 = -\frac{\partial}{\partial x_j} [\overline{\rho u_j N_c} - \bar{\rho} \tilde{u}_j \tilde{N}_c] \quad (4i)$$

$$T_2 = -\frac{2D}{\rho} \left[\overline{\dot{w} + \frac{\partial}{\partial x_j} \left(\rho D \frac{\partial c}{\partial x_j} \right)} \right] \frac{\partial c}{\partial x_i} \frac{\partial \rho}{\partial x_i} \quad (4ii)$$

$$T_3 = -2\rho D \frac{\partial c}{\partial x_i} \frac{\partial u_i}{\partial x_j} \frac{\partial c}{\partial x_j} \quad (4iii)$$

$$T_4 = \overline{2D \frac{\partial \dot{w}}{\partial x_i} \frac{\partial c}{\partial x_i}} \quad (4iv)$$

$$(-D_2) = \overline{-2\rho D^2 \frac{\partial^2 c}{\partial x_i \partial x_j} \frac{\partial^2 c}{\partial x_i \partial x_j}} \quad (4v)$$

$$f(D) = \overline{f_1(D)} = \overline{2D \frac{\partial c}{\partial x_k} \frac{\partial(\rho D)}{\partial x_k} \frac{\partial^2 c}{\partial x_j \partial x_j}} + \overline{2D \frac{\partial c}{\partial x_k} \frac{\partial^2(\rho D)}{\partial x_j \partial x_k} \frac{\partial c}{\partial x_j}} - \overline{\frac{\partial}{\partial x_j} \left(\rho N_c \frac{\partial D}{\partial x_j} \right)} \quad (4vi)$$

$$- \overline{2\rho D \frac{\partial D}{\partial x_j} \frac{\partial}{\partial x_j} \left(\frac{\partial c}{\partial x_k} \frac{\partial c}{\partial x_k} \right)} + \overline{\rho \left(\frac{\partial c}{\partial x_k} \frac{\partial c}{\partial x_k} \right) \left[\frac{\partial D}{\partial t} + u_j \frac{\partial D}{\partial x_j} \right]}$$

where \dot{w} is the reaction rate of c . The term T_1 represents the effects of sub-grid convection, whereas T_2 denotes the effects of density-variation due to heat release. The term T_3 is determined by the alignment of ∇c with local strain rate $e_{ij} = 0.5(\partial u_i / \partial x_j + \partial u_j / \partial x_i)$, and this term is commonly referred to as the scalar-turbulence interaction term. The term T_4 arises due to the correlation between $\nabla \dot{w}$ and ∇c , whereas $(-D_2)$ denotes the molecular dissipation of SDR and these terms will henceforth be referred to as the reaction rate term and dissipation term respectively. The term $f(D)$ denotes the effects of D variation. *A-priori* DNS modelling of the above unclosed terms will be discussed in Section 3 of this paper.

For the present analysis, a DNS database of freely propagating turbulent premixed flames has been considered. The simulation domain is taken to be a cube of $24.1\delta_{th} \times 24.1\delta_{th} \times 24.1\delta_{th}$ which is discretised using a uniform Cartesian grid of $230 \times 230 \times 230$ points ensuring about 10 grid points are kept within $Min(\delta_L, \delta_{th})$ where $\delta_L = 1/(Max|\nabla c|_L)$ is an alternative flame thickness based on $|\nabla c|$ and the values of δ_L / δ_{th} for cases A-E (with $Le = 0.34, 0.6, 0.8, 1.0$ and 1.2) are provided in Table 1. The initial values of the normalised root-mean-square (rms) value of turbulent velocity u' / S_L , integral length scale to thermal flame thickness ratio l / δ_{th} , Damköhler number $Da = l S_L / u' \delta_{th}$, Karlovitz number $Ka = (u' / S_L)^{3/2} (l / \delta_{th})^{-1/2}$, turbulent Reynolds number $Re_t = \rho_0 u' l / \mu_0$ and $\tau = (T_{ad} - T_0) / T_0$ are presented in Table 1 along with domain and grid sizes, where ρ_0 and μ_0 are the unburned gas density and viscosity respectively, and S_L is the unstrained laminar burning velocity. The flamelet assumption is likely to be valid for the values of u' / S_L and l / δ_{th} considered here, and all cases considered here represent the thin reaction zones regime combustion according to the regime diagram by Peters [55].

The simulations have been carried out using a well-known DNS code called SENGAs [56]. For all cases the boundary conditions in the mean flame propagation direction are taken to be partially non-reflecting, whereas boundaries in transverse directions are taken to be periodic. A 10th order central difference scheme is used for spatial differentiation for the internal grid points and the order of differentiation gradually drops to a one-sided 2nd order scheme at the non-periodic boundaries. A low-storage 3rd order Runge-Kutta method is used for explicit time advancement for all the governing equations. In all cases flame-turbulence interaction takes place under decaying turbulence, which necessitates the simulation time $t_{sim} \geq \max(t_f, t_c)$, where $t_f = l/u'$ is the initial eddy turn over time and $t_c = \alpha_{T0}/S_L^2$ is the chemical time scale with α_{T0} being the unburned gas thermal diffusivity. The simulations have been carried out for about $3.34t_f = 3.34l/u'$, which amounts to approximately $1.75\alpha_{T0}/S_L^2$ for all cases considered here. Several studies [12-15, 19, 57-61] with either similar or smaller simulation time have contributed significantly to the fundamental understanding and modelling of turbulent premixed combustion in the past. By the time the statistics were extracted, the value of u'/S_L in the unburned reactants ahead of the flame had decayed by about 50%, while the value of l/δ_{th} had increased by about 1.7 times, relative to their initial values. This database has been used in several previous analyses [20-28] and it was shown in Ref. [23] that the volume-integrated burning rate for the $Le = 1.0$ and 1.2 flames reached quasi-steady state by the time statistics were extracted. However, the $Le < 1.0$ flames are thermo-diffusively unstable and thus the volume-integrated burning rate increases with time for these cases [23]. The qualitative nature of the statistics was found to remain unchanged and the scaling estimates presented in the next section remain valid since $t = 2.0l/u'$ for all cases considered here.

The unclosed terms of the transport equation of \tilde{N}_c have been evaluated by explicitly filtering DNS data using a standard three-dimensional Gaussian filter [28, 53, 57, 58, 60]: $G(\vec{r}) = (6/\pi\Delta^2)^{3/2} \exp(-6\vec{r} \cdot \vec{r}/\Delta^2)$ and the filtered values of a general quantity Q is given by the following integral: $\overline{Q}(\vec{x}) = \int Q(\vec{x} - \vec{r})G(\vec{r})d\vec{r}$. In the next section, results will be presented for Δ ranging from $\Delta \approx 0.4\delta_{th}$ to $\Delta \approx 2.8\delta_{th}$. This range of filter widths is comparable to the range of Δ used in several previous *a-priori* DNS analyses [57, 58, 60], and address a range of different length scales from Δ comparable to $\delta_{th} \approx 1.75\delta_z$ ($\delta_z = \alpha_{T0}/S_L$ is the Zel'dovich flame thickness) up to $2.8\delta_{th} \approx 5.0\delta_z$ where Δ is comparable to the integral length scale.

3. RESULTS & DISCUSSION

The distributions of \tilde{c} on $x_1 - x_2$ mid-plane for $\Delta = 0.8\delta_{th}$, $1.6\delta_{th}$ and $2.8\delta_{th}$ at $t = t_c$ for cases A-E are shown in Fig. 1, which shows an increase in the extent of flame wrinkling with decreasing Le .

The extent of flame wrinkling can be quantified in terms of the normalised turbulent flame surface area A_T/A_L where the flame surface area is evaluated using the volume integration of the form: $A = \int_V |\nabla c| dV$ with subscripts ‘ T ’ and ‘ L ’ denoting the turbulent and laminar flame values respectively [28]. The values of A_T/A_L and the normalised turbulent burning velocity S_T/S_L (where $S_T = (\rho_0 A_p)^{-1} \int_V \dot{w} dV$) at $t_c = \delta_{th}/S_L$ are listed in Table 2, which demonstrates that both A_T/A_L and S_T/S_L increase significantly with decreasing Lewis number. The burning rate per unit area in turbulent flames increases (decreases) in comparison to the corresponding laminar value as a result of negative (positive) Markstein length [7-10] for the $Le < 1$ ($Le > 1$) flames. This, in turn, leads to $S_T/S_L > A_T/A_L$ ($S_T/S_L < A_T/A_L$) in the $Le < 1$ ($Le > 1$) flames (see Table 2). It can further be seen from Fig. 1 the flame brush thickens (i.e. the magnitude of $\nabla \tilde{c}$ decreases) and the extent of flame wrinkling decreases with increasing Δ as a result of the smearing of local information due to the convolution operation associated with LES filtering. As the SDR is related to the reaction rate, and the gradient of the reaction progress variable, the effects of Le on burning rate and Δ dependence of $\nabla \tilde{c}$ are expected to influence the statistical behaviour of SDR \tilde{N}_c and its transport. The effects of Le and Δ on the statistical behaviour of SDR \tilde{N}_c and its transport have been analysed elsewhere [28] and the current analysis will only concentrate on the influences of global Lewis number on the modelling of SDR transport.

The normalised mean values of $T_1, T_2, T_3, T_4, (-D_2)$ and $f(D)$ conditional on \tilde{c} for cases A-E are shown in Fig. 2 for $\Delta \approx 0.4\delta_{th}$ and $\Delta \approx 2.8\delta_{th}$. Figure 2 shows that T_2 and $(-D_2)$ act as source and sink respectively in all cases, which is consistent with previous findings [21,28]. The contribution of T_4 is positive for major portion of the flame brush before becoming negative towards the burned gas side for $\Delta \leq \delta_{th}$ (e.g. $\Delta \approx 0.4\delta_{th}$) but for $\Delta > \delta_{th}$ (e.g. $\Delta \approx 2.8\delta_{th}$) the contribution of T_4 remains a leading-order source throughout the flame brush. The term T_3 assumes positive values towards the unburned gas side of the flame brush before assuming mostly negative values for the major part of the flame brush in cases D and E, whereas T_3 is negative throughout the flame brush in cases A-C for all filter widths. The contribution of $f(D)$ is negative (positive) towards the unburned (burned) gas side of the flame brush for all cases and for all filter widths. The magnitude of T_1 is negligible compared to $T_2, T_3, T_4, (-D_2)$ and $f(D)$ for all Δ in all cases. It can be seen from Fig. 2 that the magnitude of the all the terms decrease with increasing Le and Δ , which is consistent with previous finding based on DNS data [22,28]. The observed behaviours of $T_1, T_2, T_3, T_4, (-D_2)$ and

$f(D)$ in response to Le and Δ have recently been explained by Gao *et al.* [28] using a detailed scaling analysis, and the scaling estimates of filtered SDR and the unclosed terms of SDR transport equation have been provided in Table 3. It is worth noting that m and n in Table 3 are positive numbers with magnitudes greater than unity, and the functions $g(Le)$, $\phi(Le)$, $\phi_1(Le)$ and $\Psi(Le)$ increase with decreasing global Lewis number Le . It can be seen from the scaling estimates in Table 3 that the magnitudes of the terms $T_1, T_2, T_3, T_4, (-D_2)$ and $f(D)$ are expected to increase with decreasing filter width and global Lewis number. Interested readers are referred to [28] for further discussion on the derivation of the scaling estimates of $T_1, T_2, T_3, T_4, (-D_2)$ and $f(D)$, and only the modelling of these terms will be discussed in this paper in the following sub-sections.

Modelling of the turbulent transport term T_1

Equation 4i indicates that the turbulent transport term T_1 could be satisfactorily closed if the sub-grid flux of SDR (i.e. $\overline{\rho u_i N_c} - \bar{\rho} \tilde{u}_i \tilde{N}_c$) is properly modelled. The sub-grid flux of SDR ($\overline{\rho u_i N_c} - \bar{\rho} \tilde{u}_i \tilde{N}_c$) is often modelled using a gradient hypothesis as [34]:

$$\left(\overline{\rho u_i N_c} - \bar{\rho} \tilde{u}_i \tilde{N}_c\right) = -\bar{\rho} D_t \frac{\partial \tilde{N}_c}{\partial x_i} \quad (5i)$$

where D_t is the sub-grid scale eddy diffusivity. It has been demonstrated earlier that the turbulent scalar flux of scalar gradients (e.g. Flame Surface Density and SDR) may exhibit counter-gradient (gradient) transport for the flames when counter-gradient (gradient) transport is observed for $(\overline{\rho u_i c} - \bar{\rho} \tilde{u}_i \tilde{c})$ [20, 22, 23, 62]. Thus, the modelling of T_1 needs to include both gradient and counter-gradient transport of $(\overline{\rho u_i N_c} - \bar{\rho} \tilde{u}_i \tilde{N}_c)$.

Gao *et al.* [28] demonstrated that the unclosed term T_1 can be scaled in the following manner:

$$T_1 \sim \frac{\rho_0 \tau g(Le) S_L \tilde{N}_c}{\Delta} \sim \frac{\rho_0 \tau g(Le) S_L^2}{\delta_{th}^2} \times Le \times Da_\Delta^{-0.5} Re_\Delta^{-0.5} \text{ for } \Delta \gg \delta_{th} \quad (5ii)$$

where $g(Le)$ is a function increasing with decreasing Le , which accounts for flame normal acceleration, S_L is used to scale the sub-grid velocity fluctuations associated with sub-grid scalar gradients, and the sub-grid fluctuations of SDR are taken to scale with S_L / δ_L [28]. In eq. 5ii, $Da_\Delta = \Delta S_L / u'_\Delta \delta_{th}$ and $Re_\Delta = \rho_0 u'_\Delta \Delta / \mu_0$ are the sub-grid Damköhler number and sub-grid turbulent Reynolds number respectively with $u'_\Delta = \sqrt{2k_{sgs}/3}$ and $k_{sgs} = (\overline{\rho u_i u_i} - \bar{\rho} \tilde{u}_i \tilde{u}_i) / 2\bar{\rho}$ being the sub-grid turbulent velocity fluctuation and sub-grid kinetic energy respectively. One obtains

$Da_\Delta \text{Re}_\Delta \sim (\Delta/\delta_{th})^2$ using $\mu_0 \sim \rho_0 S_L \delta_{th}$, which indicates that $Da_\Delta \text{Re}_\Delta$ increases with increasing Δ . Alternatively, one obtains the following expression when the sub-grid velocity fluctuations are taken to scale with u'_Δ [28]:

$$T_1 \sim \frac{\rho_0 u'_\Delta \tilde{N}_c}{\Delta} \sim \frac{\rho_0 S_L^2}{\delta_{th}^2} \times Le \times Da_\Delta^{-1} \quad \text{for } \Delta \gg \delta_{th} \quad (5iii)$$

It is worth noting that the scaling estimate given by eq. 5ii (eq. 5iii) is more appropriate for counter-gradient (gradient) transport. Equations 5ii and 5iii can be combined to obtain the following scaling estimate, which is valid for both gradient and counter-gradient transport [28]:

$$T_1 \sim \frac{(\overline{\rho u_i N_c} - \overline{\rho \tilde{u}_i \tilde{N}_c})}{\Delta} \sim \frac{(\overline{\rho u_i c} - \overline{\rho \tilde{u}_i \tilde{c}}) \tilde{N}_c}{\Delta} \quad \text{and} \quad (\overline{\rho u_i N_c} - \overline{\rho \tilde{u}_i \tilde{N}_c}) \sim (\overline{\rho u_i c} - \overline{\rho \tilde{u}_i \tilde{c}}) \tilde{N}_c \quad \text{for } \Delta \gg \delta_{th} \quad (5iv)$$

Gao *et al.* [53] have recently extended a RANS model proposed by Chakraborty and Swaminathan [51] for the purpose of modelling $(\overline{\rho u_i N_c} - \overline{\rho \tilde{u}_i \tilde{N}_c})$ for the unity Lewis number flames in the context of LES in the following manner:

$$\overline{\rho u_i N_c} - \overline{\rho \tilde{u}_i \tilde{N}_c} = \left\{ (\Phi' - \tilde{c}) \frac{\gamma_1 [\overline{\rho u_i c} - \overline{\rho \tilde{u}_i \tilde{c}}] - \gamma_2 \overline{\rho \tilde{c}} (1 - \tilde{c}) u'_\Delta M_i}{\tilde{c} (1 - \tilde{c})} \tilde{N}_c - \overline{\rho} (C_F \Delta) u'_\Delta \frac{\partial \tilde{N}_c}{\partial x_i} \right\} \quad (6i)$$

where $M_i = -(\partial \tilde{c} / \partial x_i) / |\nabla \tilde{c}|$ is the i^{th} component of the resolved flame normal vector for LES, $\Phi' = 0.7$ is a model parameter and the following values have been suggested for γ_1, γ_2 and C_F [53]:

$$\gamma_1 = 1.8, \quad \gamma_2 = 4.9 - 3.2 \text{erf}(0.15 \text{Re}_\Delta) \quad \text{and} \quad C_F = 0.11 \quad (6ii)$$

The parameterisation given by eq. 6ii ensures that γ_2 assumes an asymptotic value for large values of Re_Δ (i.e. $\text{Re}_\Delta \rightarrow \infty$). In eq. 6i, the first term on right hand side principally accounts for the effects of flame normal acceleration due to heat release, whereas the last term on right hand side of eq. 6i represents turbulent transport according to conventional gradient hypothesis. Moreover, the first and second terms on right hand side of eq. 6i are consistent with the scaling estimates given by eqs. 5iv and 5iii respectively.

The predictions of $J_{sg}^+ = (\overline{\rho u_i N_c} - \overline{\rho \tilde{u}_i \tilde{N}_c}) M_i \times \delta_{th} / \rho_0 S_L^2$ according to eq. 6i with $\Phi' = 0.7$ are compared to the corresponding quantity extracted from DNS data for $\Delta \approx 0.4\delta_{th}$, $1.6\delta_{th}$ and $2.8\delta_{th}$ in Fig. 3 for cases A-E. Figure 3 shows that even though eq. 6i predicts J_{sg}^+ in a reasonable manner in the cases with $Le \approx 1.0$ (e.g. cases C-E), this model does not adequately capture the correct qualitative and quantitative behaviours of J_{sg}^+ for the flames with $Le \ll 1.0$ (i.e. cases A and B). The model given by eqs. 6i and 6ii does not explicitly account for non-unity Lewis number effects, so it is not surprising that this model does not adequately capture the behaviour of $(\overline{\rho u_i N_c} - \overline{\rho \tilde{u}_i \tilde{N}_c})$ for

$Le \ll 1.0$ flames where the non-dimensional temperature $T^+ = (T - T_0)/(T_{ad} - T_0)$ is significantly different from the reaction progress variable c , which alters the distribution of heat release and thermal expansion within the flame brush in comparison to the $Le \approx 1.0$ flames. This behaviour is mimicked here by introducing Le dependence of the model parameter Φ' in the following manner:

$$\Phi' = 0.3(1 - Le) + 0.7 \quad (6iii)$$

The predictions of the model given by eq. 6i with Φ' according to eq. 6iii are also shown in Fig.3, which demonstrates that the model with new parameterisation $\Phi' = 0.3(1 - Le) + 0.7$ predicts J_{sg}^+ satisfactorily for all filter widths in all cases considered here and the agreement between the predictions of eq. 6i and DNS data improves with increasing Δ (see Fig. 3). The predictions of eq. 6i with Φ' according to eq. 6iii become equal to the corresponding values obtained for $\Phi' = 0.7$ for the $Le = 1.0$ case and these two predictions cannot be distinguished from each other for case D in Fig. 3. It worth noting that the sub-grid flux of reaction progress variable (i.e. $\overline{\rho u_i c} - \bar{\rho} \tilde{u}_i \tilde{c}$) requires modelling in LES, and the performances of the models for $(\overline{\rho u_i N_c} - \bar{\rho} \tilde{u}_i \tilde{N}_c)$ and the turbulent transport term T_1 depend on the modelling of $(\overline{\rho u_i c} - \bar{\rho} \tilde{u}_i \tilde{c})$. The modelling of $(\overline{\rho u_i c} - \bar{\rho} \tilde{u}_i \tilde{c})$ is beyond the scope of current analysis and interested readers are referred to a recent investigations by Chakraborty and Cant [63] and Gao *et al.*[64] for further discussion on the modelling of turbulent scalar fluxes in premixed turbulent flames.

Modelling of the density variation term T_2

For unity Lewis number flames the gas density ρ can be expressed as $\rho_0/(1 + \tau)$ [33], which leads to an alternative expression for the density variation term T_2 as [22,47,48,51,53]: $T_2 = 2\overline{(\rho \nabla \cdot \tilde{u} N_c)}$. However, $\rho = \rho_0/(1 + \tau T^+) \neq \rho_0/(1 + \tau)$ in the non-unity Lewis number flames because the equality between T^+ and c no longer holds. Although $T_2 = 2\overline{(\rho \nabla \cdot \tilde{u} N_c)}$ does not strictly hold in non-unity Lewis number flames, the gas density can still be scaled as: $\rho \sim \rho_0/(1 + \tau)$ and thus the density variation term T_2 can be scaled for adiabatic flames with low Mach number as [28]:

$$T_2 \sim 2 \left(\overline{\rho \frac{\partial u_i}{\partial x_i} N_c} \right) \sim \frac{\rho_0 \tau S_L^2}{Le^{m-1} \delta_{th}^2} \quad (7i)$$

where m is a positive number greater than unity (i.e. $m > 1$). The resolved part of T_2 can be taken to scale as [28]:

$$\begin{aligned}
(T_2)_{res} &= -\frac{2\tilde{D}}{\bar{\rho}} \left[\bar{w} + \frac{\partial}{\partial x_j} \left(\overline{\rho D \frac{\partial c}{\partial x_j}} \right) - \frac{\partial [\overline{\rho u_j c} - \bar{\rho} \tilde{u}_j \tilde{c}]}{\partial x_j} \right] \frac{\partial \tilde{c}}{\partial x_i} \frac{\partial \bar{\rho}}{\partial x_i} \\
&\sim 2\bar{\rho} \tilde{D} \nabla \tilde{c} \cdot \nabla \tilde{c} \frac{\partial \tilde{u}_i}{\partial x_i} \sim \frac{\rho_0 S_L^2}{\delta_{th}^2} \times \frac{U_{ref}}{S_L} \times Le^{-1} Re_{\Delta}^{-1.5} Da_{\Delta}^{-1.5}
\end{aligned} \tag{7ii}$$

where U_{ref} is a velocity scale representing the Favre-filtered velocity components \tilde{u}_i . It is worth noting that $\bar{\rho} = \rho_0 / (1 + \tilde{c})$ for unity Lewis number flames yields $(T_2)_{res} = 2\bar{\rho} \tilde{D} \nabla \tilde{c} \cdot \nabla \tilde{c} (\partial \tilde{u}_i / \partial x_i)$ but the expression $\bar{\rho} = \rho_0 / (1 + \tilde{c})$ does not strictly hold for non-unity Lewis number flames but $\bar{\rho}$ and $(T_2)_{res}$ can still be scaled using $\rho_0 / (1 + \tilde{c})$ and $2\bar{\rho} \tilde{D} \nabla \tilde{c} \cdot \nabla \tilde{c} (\partial \tilde{u}_i / \partial x_i)$ respectively.

The scaling estimates given by eqs. 7i and 7ii demonstrate that T_2 remains of the order of $\rho_0 \tau S_L^2 / \delta_{th}^2$ irrespective of Δ . By contrast, the magnitude of $(T_2)_{res}$ remains comparable to $\rho_0 S_L^2 / \delta_{th}^2$ for $U_{ref} \sim S_L$ and $\Delta \approx \delta_{th}$, but the magnitude of $(T_2)_{res}$ is expected to decrease with increasing Δ . This suggests that the sub-grid component $(T_2)_{sg} = T_2 - (T_2)_{res}$ plays an increasingly important role with increasing Δ , which can be substantiated from Fig. 4 where the variations of the mean values of T_2 and $(T_2)_{sg} = T_2 - (T_2)_{res}$ conditional on \tilde{c} are shown for cases A-E for $\Delta \approx 0.4\delta_{th}$, $1.6\delta_{th}$ and $2.8\delta_{th}$.

Gao *et al.* [53] recently proposed the following model T_2 for unity Le flames in the following manner:

$$T_2 = \underbrace{-\frac{2\tilde{D}}{\bar{\rho}} \left[\bar{w} + \frac{\partial}{\partial x_j} \left(\overline{\rho D \frac{\partial c}{\partial x_j}} \right) - \frac{\partial [\overline{\rho u_j c} - \bar{\rho} \tilde{u}_j \tilde{c}]}{\partial x_j} \right] \frac{\partial \tilde{c}}{\partial x_i} \frac{\partial \bar{\rho}}{\partial x_i}}_{(T_2)_{res}} + \beta_{T_2} \tau S_L \frac{[\bar{\rho} \tilde{N}_c - \bar{\rho} \tilde{D} \nabla \tilde{c} \cdot \nabla \tilde{c}]}{\delta_{th} (1.0 + Ka_{\Delta})^{1/2}} \tag{8}$$

where $Ka_{\Delta} = (u'_{\Delta} / S_L)^{3/2} (\Delta / \delta_{th})^{-1/2}$ is local sub-grid Karlovitz number and $\beta_{T_2} = 2.7$ is a model parameter. The first term on right hand side of eq. 8 accounts for the resolved component $(T_2)_{res}$ whereas the second term models the sub-grid component. The Karlovitz number dependence in eq. 8 ensures the diminishing strength of heat release with increasing Ka_{Δ} [22,28,47,48,51,52] as the combustion process is likely to show the attributes of the broken reaction zones regime [55] (where the effects of heat release are weak) for high values of Karlovitz number. The prediction of eq.8 is also shown in Fig. 4 for cases A-E for $\Delta \approx 0.4\delta_{th}$, $1.6\delta_{th}$ and $2.8\delta_{th}$. A comparison between the predictions of eq. 8 and the normalised T_2 extracted from explicitly filtered DNS data reveals that eq. 8 satisfactorily predicts T_2 for a range of

different filter widths for flames with $Le \approx 1.0$ (e.g. cases C-E) but this model significantly under-predicts the magnitude of T_2 for the $Le \ll 1.0$ cases (e.g. cases A and B). It can be seen from eq. 7i that the magnitude of T_2 is expected to increase with decreasing Le due to the strengthening of heat release effects as a result of enhanced burning rate for small values of Lewis number (see Table 2). As this effect is missing in eq. 8, this model under-predicts the magnitude of T_2 for the $Le \ll 1.0$ cases (e.g. cases A and B) where the effects of enhanced heat release due to differential diffusion of heat and mass are particularly strong.

Here the model given by eq. 8 has been extended in order to account for the effects of Le in the following manner:

$$T_2 = - \underbrace{\frac{2\tilde{D}}{\bar{\rho}} \left[\bar{\dot{w}} + \frac{\partial}{\partial x_j} \left(\overline{\rho D \frac{\partial c}{\partial x_j}} \right) - \frac{\partial [\overline{\rho u_j c} - \bar{\rho} \tilde{u}_j \tilde{c}]}{\partial x_j} \right]}_{(T_2)_{res}} \frac{\partial \tilde{c}}{\partial x_i} \frac{\partial \bar{\rho}}{\partial x_i} + f_{T_2}(Le) \frac{K_c^* S_L}{\delta_{th} (1.0 + Ka_\Delta)^{1/2}} [\bar{\rho} \tilde{N}_c - \bar{\rho} \tilde{D} \nabla \tilde{c} \cdot \nabla \tilde{c}] \quad (9i)$$

where

$$f_{T_2}(Le) = \frac{3.3}{Le^{2.57} \operatorname{erf}[4(1.0 - Le) + 1.4]} \quad \text{and} \quad K_c^* = \frac{\delta_{th}}{S_L} \frac{\int_0^1 [\rho N_c \nabla \cdot \tilde{u} f_b(c)]_L dc}{\int_0^1 [\rho N_c f_b(c)]_L dc}$$

(9ii)

In eq. 9ii $f_{T_2}(Le)$ accounts for the strengthening of heat release effects with decreasing Le as suggested by the scaling estimate given by eq. 7i. The parameter K_c^* is a thermo-chemical parameter, which provides information regarding the SDR-weighted dilatation rate $\nabla \cdot \tilde{u}$ [34, 36, 65, 66]. The thermo-chemical parameter K_c^* accounts for the correlation between $\nabla \cdot \tilde{u}$ and ρN_c within the flame front. It is possible to approximate $f_b(c)$ as: $f_b(c) = 1/|\nabla c|_L$ [65, 66], which enables one to evaluate K_c^* from laminar flame data. The thermo-chemical parameter K_c^*/τ is also affected by Le and it is equal to 0.52, 0.67, 0.71, 0.78 and 0.79 for the $Le = 0.34, 0.6, 0.8, 1.0$ and 1.2 flames considered here. The predictions of eq. 9 are compared to the predictions of eq. 8 and T_2 extracted from DNS data in Fig. 4, which shows that eq. 9 satisfactorily predicts the quantitative behaviour of T_2 for a range of different values of Δ for flames with Le ranging from 0.34 to 1.2. Equation 9 becomes exactly equal to eq. 8 for the $Le = 1.0$ case and thus the predictions of eqs. 8 and 9 cannot be distinguished from each other for case D in Fig. 4.

Modelling of the scalar turbulence interaction term T_3

The variations of the mean values of T_3 conditional on \tilde{c} are shown in Fig. 5 for cases A-E at $\Delta \approx 0.4\delta_{th}$, $1.6\delta_{th}$ and $2.8\delta_{th}$. Figure 5 shows that T_3 assumes predominantly negative values throughout the flame brush for cases A-C but this term exhibits weak positive values towards both unburned gas side of the flame brush before assuming mostly negative values for the major portion of the flame brush in cases D and E. The term T_3 can be expressed as [21, 28, 34, 45-48]:

$$T_3 = -2\rho(e_\alpha \cos^2 \alpha + e_\beta \cos^2 \beta + e_\gamma \cos^2 \gamma)N_c \quad (10)$$

where e_α , e_β and e_γ are the most extensive, intermediate and most compressive principal strain rates and their angles with ∇c respectively. Equation 10 suggests that a predominant collinear alignment of ∇c with e_α (e_γ) leads to a negative (positive) value of T_3 . It was discussed elsewhere [21, 28, 34, 45-48] that ∇c predominantly aligns with e_α when the strain rate induced by flame normal acceleration overcomes turbulent straining, whereas one obtains preferential alignment of ∇c with e_γ when turbulent straining dominates over the strain rate due to flame normal acceleration. The flame normal acceleration strengthens with decreasing Le , and thus ∇c predominantly aligns with e_α for the $Le \ll 1$ flames (e.g. cases A and B), which leads to negative values of T_3 [21, 22, 28]. By contrast, turbulent straining overcomes the flame normal acceleration on both ends of the flame brush for the $Le \approx 1.0$ cases considered here (e.g. cases C-E), which leads to positive values of T_3 both on unburned and burned gas sides of the flame brush for $\Delta \approx 0.4\delta_{th}$. However, the flame normal acceleration dominates over turbulent straining in the middle of the flame brush where the effects of heat release are strong even in the $Le \approx 1.0$ cases considered here (e.g. cases C-E), which leads to negative values of T_3 for the major portion of the flame brush in these cases.

The effects of ∇c alignment with e_α on T_3 can be scaled in the following manner [28]:

$$T_3 \sim \frac{\rho_0 \tau S_L \tilde{N}_c}{Le^n \delta_{th}} \sim \frac{\rho_0 \tau S_L^2}{Le^{n-1} \delta_{th}^2} \quad \text{where } n > 1 \quad (11i)$$

The contribution of ∇c alignment with e_γ on T_3 can be scaled as [28]:

$$T_3 \sim \frac{\rho_0 u'_\Delta \tilde{N}_c}{\Delta} \sim \frac{\rho_0 S_L^2}{\delta_{th}^2} \times Le \times Pr^{-1/2} \times Ka_\Delta \quad \text{for } \Delta \gg \delta_{th} \quad (11ii)$$

The Lewis number Le dependence in eq. 11i (with $n > 1$) accounts for greater extent of ∇c alignment with e_α for the flames with $Le \ll 1.0$. Gao *et al.* [28] proposed the following scaling estimate of the resolved part of T_3 :

$$(T_3)_{res} = -2\bar{\rho}\tilde{D} \frac{\partial\tilde{c}}{\partial x_i} \frac{\partial\tilde{u}_i}{\partial x_j} \frac{\partial\tilde{c}}{\partial x_j} \sim \frac{\rho_0 S_L^2}{\delta_{th}^2} \times \frac{U_{ref}}{S_L} \times Le^{-1} Re_\Delta^{-1.5} Da_\Delta^{-1.5} \text{ for } \Delta \gg \delta_{th} \quad (11iii)$$

A comparison of eqs. 11i-iii reveals that the contribution of $(T_3)_{res}$ to T_3 is expected to weaken with increasing Δ , and this behaviour can indeed be seen from Fig. 5, which shows that the magnitude of $(T_3)_{res}$ decreases with increasing Δ .

Gao *et al.* [53] utilised the scaling estimates given by eqs. 11i and 11ii to propose a model for T_3 for $Le = 1.0$ flames:

$$T_3 = -2\overline{\rho D} \frac{\partial\tilde{c}}{\partial x_i} \frac{\partial\tilde{u}_i}{\partial x_j} \frac{\partial\tilde{c}}{\partial x_j} + (1 - f_{T_3})(C_3 - C_4\tau \cdot Da_\Delta^*) \frac{u'_\Delta}{\Delta} \bar{\rho} \tilde{N}_c \quad (12i)$$

where C_3 and C_4 are the model parameters and $Da_\Delta^* = S_L \rho_0 \Delta / u'_\Delta \bar{\rho} \delta_{th}$ is the density-weighted local sub-grid Damköhler number. The symbol f_{T_3} is a bridging function in terms of $\Delta S_L / \alpha_{T_0}$, which ensures that $(T_3)_{sg} \approx T_3$ for $\Delta \gg \delta_{th}$ and T_3 approaches to $(T_3)_{res}$ when the flow is fully resolved:

$$\lim_{\Delta \rightarrow 0} T_3 = \lim_{\Delta \rightarrow 0} \left(-2\overline{\rho D} \frac{\partial\tilde{c}}{\partial x_i} \frac{\partial\tilde{u}_i}{\partial x_j} \frac{\partial\tilde{c}}{\partial x_j} \right) = -2\overline{\rho D} \frac{\partial\tilde{c}}{\partial x_i} \frac{\partial\tilde{u}_i}{\partial x_j} \frac{\partial\tilde{c}}{\partial x_j} \quad (12ii)$$

Gao *et al.* [53] proposed the following expressions for the model parameter C_3, C_4 and f_{T_3} :

$$C_3 = 7.5 ; C_4 = 0.75(1.0 + Ka_\Delta)^{-0.4} \text{ and } f_{T_3} = \exp[-1.05(S_L \Delta / \alpha_{T_0})^2] \quad (12iii)$$

It is worth noting that the term $C_3 \bar{\rho} (u'_\Delta / \Delta) \tilde{N}_c$ and $-C_4 \rho_0 \tau (S_L / \delta_{th}) \tilde{N}_c$ are consistent with scaling estimates given by eqs. 11ii and 11i respectively. However, a comparison between eq. 11i and $-C_4 \rho_0 \tau (S_L / \delta_{th}) \tilde{N}_c$ reveals that the increased alignment of ∇c with e_α for small values of Le as a result of the strengthening of flame normal acceleration is not accounted for by the model given by eq. 12ii. The effects of flame normal acceleration are expected to weaken with increasing Karlovitz number as the reacting flow field exhibits some attributes of passive scalar mixing for large values of Karlovitz number in the broken reaction zones regime [55]. This behaviour is mimicked here by Ka_Δ dependence of C_4 in eq. 12iii.

The predictions of eq. 12i with the model parameters given by eq. 12ii are compared to T_3 extracted from DNS data in Fig. 5, which shows that eq. 12i adequately captures the qualitative and quantitative behaviours of T_3 for the $Le \approx 1.0$ cases considered here (e.g. cases C-E) but this model has been found to under-predict the magnitude of the negative contribution of T_3 in the $Le \ll 1.0$ cases (e.g. cases A and B) for $\Delta > \delta_{th}$. It has already been noted that the increased extent of scalar gradient destruction in the $Le \ll 1.0$ flames, due to preferential alignment of ∇c with e_α under strong actions of flame normal acceleration, is not addressed

in the model given by eq. 12i. Thus, this model under-predicts the negative contribution of T_3 for the flames with $Le \ll 1.0$. Here eq. 12i has been modified in the following manner to account for non-unity Lewis number effects:

$$T_3 = -2\overline{\rho D} \frac{\partial \tilde{c}}{\partial x_i} \frac{\partial \tilde{u}_i}{\partial x_j} \frac{\partial \tilde{c}}{\partial x_j} + (1 - f_{T_3}) [C_3 - C_4 \Gamma(Le) \tau \cdot Da_\Delta^*] \frac{u'_\Delta}{\Delta} \overline{\rho} \tilde{N}_c \quad (13i)$$

where
$$\Gamma(Le) = \frac{1.7(1 - \tilde{c})^p}{Le^{2.57}} \left(\frac{\delta_L}{\delta_{th}} \right)^{1.3} \quad \text{and} \quad p = 0.2 + 1.5(1.0 - Le) \quad (13ii)$$

The involvement of the function $\Gamma(Le)$ in eq. 13i accounts for the strengthening of ∇c alignment with e_α under strong actions of flame normal acceleration in flames with small values of Lewis number. The presence of $(1 - \tilde{c})^p$ helps eq. 13i to capture the qualitative behaviour of T_3 across the flame brush. It can be seen from Fig. 5 that the model given by eq. 13i provides satisfactory qualitative and quantitative predictions of T_3 for all the flames with different values of Le for a range of Δ . It is worth noting that eq. 13i approaches eq. 12i for $Le = 1.0$ and thus the predictions of eqs. 12i and 13i cannot be distinguished from each other for case D in Fig. 5.

Modelling of the combined reaction, dissipation and diffusivity gradient contribution $[T_4 - D_2 + f(D)]$

The variations of the mean values of $[T_4 - D_2 + f(D)]$ conditional on \tilde{c} are shown in Fig.6 for A-E for $\Delta \approx 0.4\delta_{th}$, $1.6\delta_{th}$ and $2.8\delta_{th}$. It can be seen from Fig. 6 that $[T_4 - D_2 + f(D)]$ acts as a sink (source) term towards the burned (unburned) gas side of the flame brush for $\Delta \approx 0.4\delta_{th}$ and $\Delta \approx 1.6\delta_{th}$, but the mean value of $[T_4 - D_2 + f(D)]$ conditional on \tilde{c} assumes predominantly negative values for $\Delta \approx 2.8\delta_{th}$. Table 3 shows that the order of magnitudes of T_4 , $(-D_2)$ and $f(D)$ remain comparable according to the scaling analysis by Gao *et al.* [28] and their magnitudes are expected to increase with decreasing Le . Furthermore, the scaling estimates of $(T_4)_{res}$, $(-D_2)_{res}$ and $\{f(D)\}_{res}$ in Table 3 suggest that their contributions are expected to weaken with increasing Δ , where $(T_4)_{res}$, $(-D_2)_{res}$ and $\{f(D)\}_{res}$ are the resolved components of T_4 , $(-D_2)$ and $f(D)$, which are given by:

$$(T_4)_{res} = 2\tilde{D} \frac{\partial \tilde{w}}{\partial x_i} \frac{\partial \tilde{c}}{\partial x_i} \quad (14i)$$

$$(-D_2)_{res} = -2\overline{\rho} \tilde{D}^2 \frac{\partial^2 \tilde{c}}{\partial x_i \partial x_j} \frac{\partial^2 \tilde{c}}{\partial x_i \partial x_j} \quad (14ii)$$

$$\begin{aligned}
\{f(D)\}_{res} = & 2\tilde{D} \frac{\partial \tilde{c}}{\partial x_k} \frac{\partial(\bar{\rho}\tilde{D})}{\partial x_k} \frac{\partial^2 \tilde{c}}{\partial x_j \partial x_j} + 2\tilde{D} \frac{\partial \tilde{c}}{\partial x_k} \frac{\partial^2(\bar{\rho}\tilde{D})}{\partial x_j \partial x_k} \frac{\partial \tilde{c}}{\partial x_j} - \frac{\partial}{\partial x_j} \left[\bar{\rho}\tilde{D} \left(\frac{\partial \tilde{c}}{\partial x_k} \frac{\partial \tilde{c}}{\partial x_k} \right) \frac{\partial \tilde{D}}{\partial x_j} \right] \\
& - 2\bar{\rho}\tilde{D} \frac{\partial \tilde{D}}{\partial x_j} \frac{\partial}{\partial x_j} \left(\frac{\partial \tilde{c}}{\partial x_k} \frac{\partial \tilde{c}}{\partial x_k} \right) + \bar{\rho} \left(\frac{\partial \tilde{c}}{\partial x_k} \frac{\partial \tilde{c}}{\partial x_k} \right) \left[\frac{\partial \tilde{D}}{\partial t} + \tilde{u}_j \frac{\partial \tilde{D}}{\partial x_j} \right]
\end{aligned} \tag{14iii}$$

Thus, the sub-grid components $(T_4)_{sg} = T_4 - (T_4)_{res}$, $(-D_2)_{sg} = -D_2 + (D_2)_{res}$ and $\{f(D)\}_{sg} = f(D) - \{f(D)\}_{res}$ are expected to play major roles for $\Delta \gg \delta_{th}$. The aforementioned behaviours of the resolved and sub-grid components of T_4 , $(-D_2)$ and $f(D)$ can be confirmed from Fig. 6. It can be seen from Table 3 that the magnitudes of $(T_4)_{sg}$, $(-D_2)_{sg}$ and $\{f(D)\}_{sg}$ remain of the order of $\rho_0 S_L^2 / \delta_{th}^2 \sim \bar{\rho} \tilde{N}_c^2$ for $\Delta \gg \delta_{th}$ but their magnitudes are expected to increase with decreasing Le , which can indeed be substantiated from Fig. 6.

Gao *et al.* [53] utilised $\{T_4 - D_2 + f(D)\}_{sg} \sim \rho_0 S_L^2 / \delta_{th}^2 \sim \bar{\rho} \tilde{N}_c^2$ to model $[T_4 + f(D) - D_2]$ together for unity Lewis number flames by extending an existing RANS model [22,34,44,47,48,51] in the following manner:

$$T_4 - D_2 + f(D) = (T_4)_{res} - (D_2)_{res} + \{f(D)\}_{res} - (1 - f_{TD}) \beta_3 (\tilde{c} - c^*) \bar{\rho} \frac{[\tilde{N}_c - \tilde{D} \nabla \tilde{c} \cdot \nabla \tilde{c}]^2}{\tilde{c}(1 - \tilde{c})} \tag{15i}$$

$$\text{where } \beta_3 = 5.7; c^* = 1.0 - 0.83 \operatorname{erf} \left[0.5 \frac{\Delta S_L}{\alpha_{T0}} - 2.3 \right] \text{ and } f_{TD} = \exp \left[-0.27 \left(\frac{\Delta S_L}{\alpha_{T0}} \right)^{1.7} \right] \tag{15ii}$$

The involvement of $(\tilde{c} - c^*) / [\tilde{c}(1 - \tilde{c})]$ in eq. 15i is required for capturing the qualitative behaviour of $[T_4 - D_2 + f(D)]$ across the flame brush, whereas f_{TD} approaches unity for small values of Δ as the terms get fully resolved (i.e. $\lim_{\Delta \rightarrow 0} [T_4 - D_2 + f(D)] = \lim_{\Delta \rightarrow 0} [(T_4)_{res} - (D_2)_{res} + \{f(D)\}_{res}]$). The transition from positive to negative contribution of $[T_4 + f(D) - D_2]$ with increasing Δ has been accounted for by c^* . The predictions of eq. 15i are shown in Fig. 6, which show that this model captures both the qualitative and quantitative behaviours of $[T_4 + f(D) - D_2]$ for the $Le \approx 1.0$ cases considered here (e.g. case C-E) but this model under-predicts the magnitude of $[T_4 + f(D) - D_2]$ significantly for the $Le \ll 1.0$ cases (e.g. cases A and B). It is worth noting that the model given by eq. 15i does not account for the increased magnitude of $\{T_4 - D_2 + f(D)\}_{sg}$ for small values of Le (see Table 3) so perhaps it is not surprising that this model under-predicts the magnitude of $[T_4 + f(D) - D_2]$ for the flames with $Le \ll 1.0$ (e.g. cases A and B). The increased magnitude of $[T_4 + f(D) - D_2]$ for small values of Le is accounted for by modifying eq. 15i in the following manner:

$$T_4 - D_2 + f(D) = (T_4)_{res} - (D_2)_{res} + \{f(D)\}_{res} - (1 - f_{TD})\beta'_3(\tilde{c} - c^*)\bar{\rho} \frac{[\tilde{N}_c - \tilde{D}\nabla\tilde{c} \cdot \nabla\tilde{c}]^2}{\tilde{c}(1 - \tilde{c})} \quad \text{with } \beta'_3 = 5.7Le^{-0.2} \quad (16)$$

where c^* and f_{TD} are taken according to eq. 15ii. The predictions of eq.16 are shown in Fig. 6, which demonstrates that eq.16 captures both the qualitative and quantitative behaviours of $[T_4 + f(D) - D_2]$ for a range of filter widths for different Le cases considered here. Equations 15i and 16 become equal to each other for $Le = 1.0$ and thus their predictions cannot be separated from each other in case D in Fig. 6.

It is worth noting that the combined contribution of the terms D_1 , T_4 , $f(D)$ and $(-D_2)$ can be expressed in the following manner if the SDR transport equation is derived based on the kinematic form of the progress variable transport equation (i.e. $Dc/Dt = S_d|\nabla c|$) [34,47]:

$$D_1 + T_4 - D_2 + f(D) \approx -2D\nabla \cdot (\rho S_d \bar{n} |\nabla c|) |\nabla c| + 2D\rho S_d \nabla \cdot \bar{n} |\nabla c|^2 \quad (17)$$

where $S_d = [\dot{w} + \nabla \cdot (\rho D \nabla c)] / (\rho |\nabla c|)$ and $\bar{n} = -\nabla c / |\nabla c|$ are the flame displacement speed and local flame normal vector respectively. Thus, eq. 17 suggests that the net contribution of $[T_4 - D_2 + f(D)]$ originates due to flame normal propagation and flame curvature. This justifies modelling these terms together [21, 34, 44, 47, 48, 53] because the molecular diffusion term D_1 is a closed term. Although eq. 16 reasonably captures the qualitative behaviour and the magnitude of $[T_4 + f(D) - D_2]$ for all cases considered here, the collective modelling of the terms T_4 , $f(D)$ and $(-D_2)$ may give rise to the loss of their individual physical significances. However, this is one of the first attempts to model the Lewis number effects on the SDR transport equation terms in the context of LES of premixed combustion and thus there is a scope for further improvement of this modelling in the future.

Implications of model implementation

The newly proposed models for the unclosed terms of the SDR \tilde{N}_c transport equation are summarised in Table 4 for the future potential users of these models. It is worth noting that the flamelet assumption is invoked while deriving these models so they are expected to remain valid in the corrugated flamelets and thin reaction zones regimes of turbulent premixed combustion [55]. The scaling estimates in Table 3 indicate that the terms $T_2, T_3, T_4, (-D_2)$ and $f(D)$ remain leading order contributors to the SDR \tilde{N}_c transport and the magnitude of T_1 remains negligible in comparison to the terms $T_2, T_3, T_4, (-D_2)$ and $f(D)$ irrespective of Damköhler and turbulent Reynolds numbers. This is consistent with the observations made from Fig. 2. However, the turbulent transport term T_1 still need to be modelled and included in the model implementation for LES for numerical stability.

4. CONCLUSIONS

The effects of global Lewis number Le on the modelling of the unclosed terms of the transport equation of Favre-filtered SDR \tilde{N}_c have been analysed based on *a-priori* analysis of a DNS database of freely propagating statistically planar turbulent premixed flames with Le ranging from 0.34 to 1.2. It has been found that Le has profound influence on the statistical behaviour of the unclosed terms of \tilde{N}_c transport arising from turbulent transport T_1 , density variation due to heat release T_2 , alignment of scalar and velocity gradients T_3 , correlation between the gradients of reaction rate and reaction progress variable T_4 , molecular dissipation ($-D_2$) and diffusivity gradients $f(D)$ and detailed physical explanations have been provided for the observed non-unity Lewis number effects. Recently proposed models for $T_1, T_2, T_3, T_4, (-D_2)$ and $f(D)$ for unity Lewis number flames have been extended here to account for the effects of Le based on the scaling estimates of these unclosed terms [28]. The newly proposed models have been found to satisfactorily predict the unclosed terms obtained from explicitly filtered DNS data for a range of Δ for different values of Le . However, it is still essential to implement these models into actual LES simulations for the purpose of *a-posteriori* assessment. Moreover, these models need to be further validated based on detailed chemistry based DNS simulations. Further validation of these models will form the basis of future investigations.

ACKNOWLEDGEMENTS

The financial assistance of the Engineering and Physical Science (EPSRC) research council of the UK (EP/I028013/1) and computational support of N8 are gratefully acknowledged.

REFERENCES

1. Huang, Y., Yang, V., Dynamics and stability of lean-premixed swirl stabilised combustion, *Prog. Energy Combust. Sci.*, vol. **35**(4), pp. 293-364, 2009.
2. Wallner, T., Ng, H. K., Peters, R.W., The effects of blending hydrogen with methane on energy operation, efficiency and emissions, *Proc. SAE Trans.*, 2007-01-0474, 2007.
3. Schefer, R., Reduced turbine emissions using hydrogen-enriched fuels, *Proc. of the 2002 U.S. DOE Hydrogen Program Review NREL/CP-610-32405*, 2002.
4. Mizomoto, M., Asaka, S., Ikai, S. and Law, C.K., Effects of preferential diffusion on the burning intensity of curved flames, *Proc. Combust. Inst.*, vol. **20**, pp. 1933-1939, 1984.
5. Law, C.K., Kwon, O.C., Effects of hydrocarbon substitution on atmospheric hydrogen-air flame propagation, *Int. J. Hydrogen Energy*, vol. **29**, pp. 867-879, 2004.
6. Dinkelacker, F., Manickam, B., Muppala, S.R., Modelling and Simulation of lean premixed turbulent methane/hydrogen/air flames with an effective Lewis number approach, *Combust. Flame*, vol. **158**, pp. 1742-1749, 2011.

7. Pelce, P., Clavin, P., Influence of hydrodynamics and diffusion upon the stability limits of laminar premixed flames, *J. Fluid Mech.*, vol. **124**, pp. 219-237, 1982.
8. Clavin P., Williams, F.A., Effects of molecular diffusion and thermal expansion on the structure and dynamics of turbulent premixed flames in turbulent flows of large scale and small intensity, *J. Fluid Mech.*, vol. **128**, pp. 251-282, 1982.
9. Libby, P.A., Linan, A., Williams, F.A., Strained premixed laminar flames with non-unity Lewis numbers, *Combust. Sci. Technol.*, vol. **34**, 257-293, 1983.
10. Sivashinsky, G.I., Instabilities, Pattern Formation and Turbulence in Flames, *Annu. Rev. Fluid Mech.*, vol. **15**, pp. 179-190, 1983.
11. Abdel-Gayed, R.G., Bradley, D., Hamid, M., Lawes, M., Lewis number effects on turbulent burning velocity, *Proc. Combust. Inst.*, vol. **20**, pp. 505-512, 1984.
12. Ashurst, W.T., Peters, N., Smooke, M.D., Numerical Simulation of Turbulent Flame Structure with non-unity Lewis number, *Combust. Sci. Technol.*, vol. **53**, pp. 339-375, 1987.
13. Haworth, D., Poinso, T. J., Numerical simulations of Lewis number effects in turbulent premixed flames), *J. Fluid Mech.*, vol. **244**, pp. 405-436, 1992.
14. Rutland, C. J., Trouvé, A., Direct Simulations of Premixed Turbulent Flames with Nonunity Lewis numbers, *Combust. Flame*, vol. **94**, pp. 41-57, 1993.
15. Trouvé, A., Poinso, T. J., The evolution equation for flame surface density in turbulent premixed combustion, *J. Fluid Mech.*, vol. **278**, pp. 1-31, 1994.
16. Chakraborty, N., Cant, R. S., Influence of Lewis Number on Curvature Effects in Turbulent Premixed Flame Propagation in the Thin Reaction Zones Regime, *Phys. Fluids*, vol. **17**, 105105, 2005.
17. Yuan, J., Ju, Y., Law, C. K., Coupled hydrodynamic and diffusional thermal instabilities in flame propagation at small Lewis numbers, *Phys. Fluids*, vol. **17**, 074106, 2005.
18. Chakraborty, N., Klein, M., A Priori Direct Numerical Simulation assessment of algebraic Flame Surface Density models for turbulent premixed flames in the context of Large Eddy Simulation. *Phys. Fluids*, vol. **20**, 085108, 2008.
19. Han, I., Huh, K.H., Roles of displacement speed on evolution of flame surface density for different turbulent intensities and Lewis numbers in turbulent premixed combustion, *Combust. Flame.*, vol. **152**, pp. 194-205, 2008.
20. Chakraborty, N., Cant, R.S., Effects of Lewis number on scalar transport in turbulent premixed flames, *Phys. Fluids.*, vol. **21**, 035110, 2009.
21. Chakraborty, N., Klein, M., Swaminathan, N., Effects of Lewis number on reactive scalar gradient alignment with local strain rate in turbulent premixed flames, *Proc. Combust. Inst.*, vol. **32**, pp. 1409-1417, 2009.
22. Chakraborty, N., Swaminathan, N., Effects of Lewis number on scalar dissipation transport and its modelling implications for turbulent premixed combustion, *Combust. Sci. Technol.*, vol. **182**, pp. 1201-1240, 2010.

23. Chakraborty, N., Cant, R.S., Effects of Lewis number on Flame Surface Density transport in turbulent premixed combustion, *Combust. Flame*, vol. **158**, pp. 1768-1787, 2011.
24. Chakraborty, N., Katragadda, M., Cant, R.S., Effects of Lewis number on turbulent kinetic energy transport in turbulent premixed combustion, *Phys. Fluids*, vol. **23**, 075109, 2011.
25. Chakraborty, N. and Swaminathan, N., Effects of Lewis number on scalar variance transport in turbulent premixed flames. *Flow, Turb. Combust.*, vol. **87**(2-3), pp. 261-292, 2011.
26. Chakraborty, N., Lipatnikov, A.N., Effects of Lewis number on the statistics of conditional fluid velocity in turbulent premixed combustion in the context of Reynolds Averaged Navier Stokes simulations, *Phys. Fluids*, vol. **25**, 045101, 2013.
27. Chakraborty, N., Wang, L., Klein, M., Effects of Lewis number on streamline segment analysis of turbulent premixed flames, *Phys. Rev. E*, vol. **89**, 033015, 2014.
28. Gao, Y., Chakraborty, N. and Swaminathan, N., Scalar Dissipation Rate Transport in the Context of Large Eddy Simulations for Turbulent Premixed Flames with Non-Unity Lewis Number, *Flow Turb. Combust.*, vol. **93**, pp. 461-486, 2014.
29. Bilger, R.W., Some aspects of scalar dissipation, *Flow Turb. Combust.*, vol. **72**, pp. 93-114, 2004.
30. Fox, R.O.: Computational models for turbulent reacting flow, Cambridge University Press, 2003.
31. Kasagi, N., Tomita, Y., Kuroda, A., Direct Numerical Simulation of passive scalar field in a turbulent channel flow, *J. Heat Transfer*, vol. **114**(3), pp. 598-606, 2008.
32. Cheung, S.C.P., Yeoh, G.H., Cheung, A.L.K., Yuen, R.K.K., Lo, S.M.: Flickering behaviour of turbulent fires using Large Eddy Simulation, *Numer. Heat Trans. A.*, vol. **52**(7), pp. 679-712, 2007.
33. Bray, K.N.C.: Turbulent flows with premixed reactants, in Libby, P.A. and Williams, F.A. (Eds.) *Turbulent Reacting Flows*, Springer Verlag, Berlin Heidelberg, New York, pp. 115-183, 1980.
34. Chakraborty, N., Champion, M., Mura, A., Swaminathan, N., Scalar dissipation rate approach to reaction rate closure, Turbulent premixed flame, (Eds. N. Swaminathan, K.N.C. Bray), Cambridge University Press, 1st Edition, Cambridge, UK, pp. 76-1023, 2011.
35. Malkeson, S.P., Chakraborty, N.: The modeling of fuel mass fraction variance transport in turbulent stratified flames: A Direct Numerical Simulation study, *Numer. Heat Trans. A.*, vol. **58**(3), pp. 187-206, 2010.
36. Dunstan, T., Minamoto, Y., Chakraborty, N., Swaminathan, N.: Scalar dissipation rate modelling for Large Eddy Simulation of turbulent premixed flames, *Proc. Combust. Inst.* vol. **34**, pp.1193-1201, 2013.
37. Gao, Y., Chakraborty, N., Swaminathan, N.: Algebraic closure of scalar dissipation rate for Large Eddy Simulations of turbulent premixed combustion, *Combust. Sci. Technol.*, vol. **186**, pp. 1309-1337, 2014.
38. Ma, T., Gao, Y., Kempf, A.M., Chakraborty, N., Validation and Implementation of algebraic LES modelling of Scalar Dissipation Rate for reaction rate closure in turbulent premixed combustion. *Combust. Flame*, vol. **161**, pp. 3134-3153, 2014.
39. Raju, M.S., Application of scalar Monte-Carlo probability density function method for turbulent spray flames, *Numer. Heat Trans. A.*, vol. **30**(8), pp. 753-777, 1996.

40. Pei, Y., Hawkes, E.R., Kook, S., Transported probability density function modelling of the vapour phase of an n-heptane jet at diesel engine conditions, *Proc. Combust. Inst.*, vol. **34**, pp. 3039-3047, 2013.
41. Pei, Y., Hawkes, E.R., Kook, S., A comprehensive study of effects of mixing and chemical kinetic models on predictions of n-heptane jet ignitions with the PDF method, *Flow, Turb Combust.*, vol. **91**, pp. 249-280, 2013.
42. Mantel, T., Borghi, R., New model of premixed wrinkled flame propagation based on a scalar dissipation equation, *Combust. Flame*, **96** (4), pp. 443-457, 1994.
43. Mura, A., Borghi, R., Towards an extended scalar dissipation equation for turbulent premixed combustion. *Combust. Flame*, vol. **133**, pp. 193-196, 2003.
44. Swaminathan, N., Bray, K.N.C., Effect of dilatation on scalar dissipation in turbulent premixed flames, *Combust. Flame*, vol. **143**, pp. 549-565, 2005.
45. Chakraborty, N., Swaminathan, N., Influence of Damköhler number on Turbulence-Scalar interaction in Premixed Flames, Part I: Physical Insight, *Phys. Fluids*, vol. **19**, 045103, 2007.
46. Chakraborty, N., and Swaminathan, N., Influence of Damköhler number on Turbulence-Scalar interaction in Premixed Flames, Part II: Model Development., *Phys. Fluids.*, vol. **19**, 045104, 2007.
47. Chakraborty, N., Rogerson, J.W., and Swaminathan, N., *A Priori* assessment of closures for scalar dissipation rate transport in turbulent premixed flames using direct numerical simulation, *Phys. Fluids.*, vol. **20**, 045106, 2008.
48. Chakraborty, N., Rogerson, J.W, and Swaminathan, N., The scalar gradient alignment statistics of flame kernels and its modelling implications for turbulent premixed combustion, *Flow Turb. Combust.*, vol. **85**, pp.25-55, 2010.
49. Mura, A., Tsuboi, K., and Hasegawa, T., Modelling of the correlation between velocity and reactive scalar gradients in turbulent premixed flames based on DNS data. *Combust. Theor. Modell.*, vol. **12**, pp. 671-698, 2008.
50. Mura, A., Robin, V, Champion, M., Hasegawa, T., Small-scale features of velocity and scalar fields of turbulent premixed flames. *Flow Turb. Combust.*, vol. **82**, pp. 339-358, 2009.
51. Chakraborty, N., Swaminathan, N.. Effects of turbulent Reynolds number on the Scalar Dissipation Rate transport in turbulent premixed flames in the context of Reynolds Averaged Navier Stokes simulations, *Combust. Sci. Technol.*, vol. **185**, pp. 676-709, 2013.
52. Knudsen, E., Richardson, E.S., Doran, E.M., Pitsch, H. Chen, J.H., Modeling scalar dissipation and scalar variance in large eddy simulation: Algebraic and transport equation closures *Phys. Fluids*, vol. **24**, 055103, 2012.
53. Gao, Y., Chakraborty, N. and Swaminathan, N.: Scalar dissipation rate transport and its modelling for Large Eddy Simulations of turbulent premixed combustion. *Combust. Sci. Technol.*, vol. **187**, 3, pp. 362-383, 2015.

54. Chen, J.H., Choudhary, A., and De Supinski, D., Hawkes, E. R., Klasky, S., Liao, W. K., Ma, K. L., Mellor-Crummey, J., Podhorski, N., Sankaran, R., Shende, S., Yoo, C. S., Terascale direct numerical simulations of turbulent combustion using S3D, *Comput. Sci. Discov.*, vol. **2**, 1, 015001, 2009.
55. Peters, N., *Turbulent Combustion*, Cambridge University Press, Cambridge, UK, 2000.
56. Jenkins K.W. Cant, R.S., DNS of turbulent flame kernels in (Eds. Liu, C, Sakell, L., Beautner, T.) *Proc. Second AFOSR Conf. on DNS and LES*, Kluwer Academic Publishers, pp. 191-202, 1999.
57. Boger, M., Veynante, D., Boughanem, H., Trouvé, A., Direct Numerical Simulation analysis of flame surface density concept for Large Eddy Simulation of turbulent premixed combustion. *Proc. Combust. Inst.*, vol. **27**, pp. 917-925, 1998.
58. Charlette, F., Meneveau, C., Veynante, D., A power-law flame wrinkling model for LES of premixed turbulent combustion. Part I: non-dynamic formulation and initial tests. *Combust. Flame*, vol. **131**, pp.159–180, 2002.
59. Grout, R.W., An Age-extended Progress Variable for Conditioning Reaction Rates, *Phys. Fluids*, vol.**19**, 105107, 2007.
60. Reddy, H. and Abraham, J., Two-Dimensional Direct Numerical Simulation Evaluation of the Flame Surface Density Model for Flames Developing from an Ignition Kernel in Lean Methane/Air Mixtures Under Engine Conditions, *Phys. Fluids*, vol. **24**,105108, 2012.
61. Pera, C., Chevillard, S., Reveillon, J., Effects of residual burnt gas heterogeneity on early flame propagation and on cyclic variability in spark-ignited engines, *Combust. Flame*, vol. **160**, pp. 1020-1032, 2013.
62. Veynante, D., Trouvé, A., Bray, K.N.C., Mantel, T., Gradient and countergradient turbulent scalar transport in turbulent premixed flames. *J. Fluid Mech.*, vol. **332**, pp. 263-293, 1997.
63. Chakraborty, N., Cant, R.S., Effects of turbulent Reynolds number on turbulent scalar flux modelling in premixed flames using Reynolds Averaged Navier-Stokes Simulations, *Numer. Heat Trans. A.*, vol. **67**(11), pp. 1187-1207, 2015.
64. Gao, Y., Chakraborty, N., Klein M., Assessment of the performances of sub-grid scalar flux models for premixed flames with different global Lewis numbers: A Direct Numerical Simulation analysis, *Int. J. Heat and Fluid Flow*, vol. **52**, pp. 28-39, 2015.
65. Kolla, H., Rogerson, J., Chakraborty, N., Swaminathan, N., Prediction of turbulent flame speed using scalar dissipation rate, *Combust. Sci. Technol.*, vol. **181**, pp. 518-535, 2009.
66. Rogerson, J.W., Swaminathan, N.: Correlation between dilatation and scalar dissipation in turbulent premixed flames, *Proc. 3rd European Combustion Meeting* Crete, Chaina, Greece, 11th to 13th April, 2007.

TABLES

Case	Le	u'/S_L	δ_L/δ_{th}	l/δ_{th}	τ	Re_t	Da	Ka
A	0.34	7.5	2.17	2.45	4.5	47.0	0.33	13.0
B	0.6	7.5	1.40	2.45	4.5	47.0	0.33	13.0
C	0.8	7.5	1.15	2.45	4.5	47.0	0.33	13.0
D	1.0	7.5	1.0	2.45	4.5	47.0	0.33	13.0
E	1.2	7.5	0.90	2.45	4.5	47.0	0.33	13.0

For all cases $\tau = 4.5$; $\beta = 6.0$; $Pr = 0.7$; $Ma = S_L / \sqrt{\gamma RT_0} = 0.014159$

Table 1: Initial values of simulation parameters and non-dimensional numbers relevant to DNS database considered for this analysis.

Case	A_T / A_L	S_T / S_L
A	3.93	13.70
B	2.66	4.58
C	2.11	2.53
D	1.84	1.83
E	1.76	1.50

Table 2: The effects of Lewis number on normalised flame surface area A_T / A_L and normalised turbulent flame speed S_T / S_L when the statistics were extracted (i.e. $t = 1.75\alpha_{T0} / S_L^2$).

Quantities	Scaling estimates
\tilde{N}_c	$\frac{S_L}{\delta_L}$
$\tilde{D}\nabla\tilde{c}\cdot\nabla\tilde{c}$	$\frac{S_L}{\delta_L} Le^{-2} Re_{\Delta}^{-1} Da_{\Delta}^{-1}$
T_1	$\frac{\tau g_2(Le)\rho_0 S_L^2}{\delta_{th}^2} \times Le \times Da_{\Delta}^{-0.5} Re_{\Delta}^{-0.5}$ alternatively $\frac{\rho_0 S_L^2}{\delta_{th}^2} \times Le \times Da_{\Delta}^{-1}$ The above expressions can be combined as $\frac{(\rho u_i c - \bar{\rho} \tilde{u}_i \tilde{c}) \tilde{N}_c}{\Delta}$
T_2	$\frac{\tau \rho_0 S_L^2}{Le^{m-1} \delta_{th}^2}$
$(T_2)_{res}$	$\frac{\rho_0 S_L^2}{\delta_{th}^2} \times \frac{U_{ref}}{S_L} \times Le^{-1} Re_{\Delta}^{-1.5} Da_{\Delta}^{-1.5}$
T_3	$\frac{\tau \rho_0 S_L^2}{Le^{n-1} \delta_{th}^2}$ alternatively $\frac{\rho_0 S_L^2}{\delta_{th}^2} \times Le \times Pr^{-1/2} \times Ka_{\Delta}$
$(T_3)_{res}$	$\frac{\rho_0 S_L^2}{\delta_{th}^2} \times \frac{U_{ref}}{S_L} \times Le^{-1} Re_{\Delta}^{-1.5} Da_{\Delta}^{-1.5}$
T_4	$\frac{\phi(Le)\rho_0 S_L^2}{\delta_{th}^2}$
$(T_4)_{res}$	$\frac{\phi_1(Le)\rho_0 S_L^2}{\delta_{th}^2} \times Re_{\Delta}^{-1} Da_{\Delta}^{-1} Le^{-1}$
$(-D_2)$	$\frac{\rho_0 \Psi(Le)^2 S_L^2}{\delta_{th}^2} \times Le^{-2}$ alternatively $(-D_2) \sim \frac{\rho_0 S_L^2}{\delta_{th}^2} \times \frac{Ka_{\Delta}^2}{Pr^3 Le^2}$
$(-D_2)_{res}$	$\frac{\rho_0 S_L^2}{\delta_{th}^2} \times Le^{-2} Re_{\Delta}^{-2} Da_{\Delta}^{-2}$
$f(D)$	$\frac{\rho_0 \tau S_L^2}{Le^{m-1} \delta_{th}^2}$
$\{f(D)\}_{res}$	$\frac{\rho_0 S_L^2}{\delta_{th}^2} \times Le^{-2} Re_{\Delta}^{-2} Da_{\Delta}^{-2}$

Table 3: Summary of the scaling estimates of the relevant quantities according to Gao *et al.*[28].

Term	Model expression
$[\overline{\rho u_i N_c} - \overline{\rho \tilde{u}_i \tilde{N}_c}]$	$[\overline{\rho u_i N_c} - \overline{\rho \tilde{u}_i \tilde{N}_c}] = (\Phi - \tilde{c}) \frac{\gamma_1 [\overline{\rho u_i c} - \overline{\rho \tilde{u}_i \tilde{c}}] - \gamma_2 \overline{\rho \tilde{c}} (1 - \tilde{c}) u'_\Delta M_i}{\tilde{c} (1 - \tilde{c})} \tilde{N}_c$ $- \overline{\rho} (C_F \Delta) u'_\Delta \frac{\partial \tilde{N}_c}{\partial x_i}$ <p>where $\gamma_1 = 1.8$, $\gamma_2 = 4.9 - 3.2 \text{erf}(0.15 \text{Re}_{i\Delta})$, $\text{Re}_{i\Delta} = \rho_0 u'_\Delta \Delta / \mu_0$, $\Phi = 0.3(Le - 1) + 0.7$ and $C_F = 0.11$</p>
T_2	$T_2 = -\frac{2\tilde{D}}{\overline{\rho}} \left[\overline{\tilde{w}} + \frac{\partial}{\partial x_j} \left(\overline{\rho D} \frac{\partial \tilde{c}}{\partial x_j} \right) - \frac{\partial [\overline{\rho u_j c} - \overline{\rho \tilde{u}_j \tilde{c}}]}{\partial x_j} \right] \frac{\partial \tilde{c}}{\partial x_i} \frac{\partial \overline{\rho}}{\partial x_i}$ $+ \frac{K_c^* f_{T_2}(Le) S_L}{(1.0 + Ka_\Delta)^{1/2} \delta_{th}} [\overline{\rho \tilde{N}_c} - \overline{\rho \tilde{D} \nabla \tilde{c}} \cdot \nabla \tilde{c}]$ <p>where $Ka_\Delta = (u'_\Delta / S_L)^{3/2} (\Delta / \delta_{th})^{-1/2}$ is local sub-grid Karlovitz number and</p> $f_{T_2}(Le) = \frac{3.3}{Le^{2.57} \text{erf}[4(1.0 - Le) + 1.4]}.$
T_3	$T_3 = -2\overline{\rho D} \frac{\partial \tilde{c}}{\partial x_i} \frac{\partial \tilde{u}_i}{\partial x_j} \frac{\partial \tilde{c}}{\partial x_j} + (1 - f_{T_3}) [C_3 - C_4 \Gamma(Le) \tau \cdot Da_\Delta^*] \frac{u'_\Delta}{\Delta} \overline{\rho \tilde{N}_c}$ <p>where $C_3 = 7.5$, $C_4 = 0.75(1.0 + Ka_\Delta)^{-0.4}$, $f_{T_3} = \exp[-1.05(\Delta S_L / \alpha_{T0})^2]$ and $Da_\Delta^* = S_L \rho_0 \Delta / u'_\Delta \overline{\rho} \delta_{th}$</p> $\Gamma(Le) = \frac{1.7(1 - \tilde{c})^p}{Le^{2.57}} \left(\frac{\delta_L}{\delta_{th}} \right)^{1.3} \text{ with } p = 0.2 + 1.5(1 - Le)$
$[T_4 - D_2 + f(D)]$	$T_4 - D_2 + f(D) = (T_4)_{res} - (D_2)_{res} + \{f(D)\}_{res}$ $- (1 - f_{TD}) \beta'_3 \overline{\rho} (\tilde{c} - c^*) \frac{[\tilde{N}_c - \tilde{D} \nabla \tilde{c} \cdot \nabla \tilde{c}]^2}{\tilde{c} (1 - \tilde{c})}$ <p>where $(T_4)_{res} = 2\tilde{D} \frac{\partial \overline{\tilde{w}}}{\partial x_i} \frac{\partial \tilde{c}}{\partial x_i}$, $(-D_2)_{res} = -2\overline{\rho \tilde{D}}^2 \frac{\partial^2 \tilde{c}}{\partial x_i \partial x_j} \frac{\partial^2 \tilde{c}}{\partial x_i \partial x_j}$,</p> $\{f(D)\}_{res} = 2\tilde{D} \frac{\partial \tilde{c}}{\partial x_k} \frac{\partial (\overline{\rho \tilde{D}})}{\partial x_k} \frac{\partial^2 \tilde{c}}{\partial x_j \partial x_j} + 2\tilde{D} \frac{\partial \tilde{c}}{\partial x_k} \frac{\partial^2 (\overline{\rho \tilde{D}})}{\partial x_j \partial x_k} \frac{\partial \tilde{c}}{\partial x_j} - \frac{\partial}{\partial x_j} \left[\overline{\rho \tilde{D} \nabla \tilde{c}} \cdot \nabla \tilde{c} \frac{\partial \tilde{D}}{\partial x_j} \right],$ $- 2\overline{\rho \tilde{D}} \frac{\partial \tilde{D}}{\partial x_j} \frac{\partial (\nabla \tilde{c} \cdot \nabla \tilde{c})}{\partial x_j} + \overline{\rho \tilde{c}} \cdot \nabla \tilde{c} \left[\frac{\partial \tilde{D}}{\partial t} + \tilde{u}_j \frac{\partial \tilde{D}}{\partial x_j} \right]$ <p>$f_{TD} = \exp[-0.27(S_L \Delta / \alpha_{T0})^{1.7}]$, $c^* = 1.0 - 0.83 \text{erf}[0.5(\Delta S_L / \alpha_{t0}) - 2.3]$ and $\beta'_3 = 5.7 / Le^{0.2}$</p>

Table 4: Summary of the proposed models for the unclosed terms of the SDR \tilde{N}_c transport equation (eq. 3) in this analysis.

FIGURE CAPTIONS

Figure 1: Distributions of \tilde{c} on $x_1 - x_2$ mid-plane for $\Delta = 0.8\delta_{th}$ (1st column); $1.6\delta_{th}$ (2nd column); $2.8\delta_{th}$ (3rd column) for cases A-E (1st -5th row) when the statistics were extracted (i.e. $t = 1.75\alpha_{T0} / S_L^2$).

Figure 2: Variations of T_1 (—), T_2 (- - - -), T_3 (—*—), T_4 (—□—), $(-D_2)$ (—△—) and $f(D)$ (—+—) conditionally averaged in bins of \tilde{c} for $\Delta \approx 0.4\delta_{th}$ (1st column), $1.6\delta_{th}$ (2nd column) and $2.8\delta_{th}$ (3rd column) in cases A-E (1st -5th row). All the terms are normalised with respect to $\rho_0 S_L^2 / \delta_{th}^2$.

Figure 3: Variations of $J_{sg}^+ = (\overline{\rho u_i N_c} - \overline{\rho \tilde{u}_i \tilde{N}_c}) M_i \times \delta_{th} / \rho_0 S_L^2$ (—) conditionally averaged in bins of \tilde{c} along with the predictions of eqs. 6i and 6ii with $\Phi' = 0.7$ (—×—) and eq. 6i and 6ii with Φ' according to eq. 6iii (- - - -) for $\Delta \approx 0.4\delta_{th}$ (1st column), $1.6\delta_{th}$ (2nd column) and $2.8\delta_{th}$ (3rd column) in cases A-E (1st -5th row).

Figure 4: Variations of T_2 (—) and $(T_2)_{sg}$ (—●—) conditionally averaged in bins of \tilde{c} along with the predictions of eq.8 (—×—) and eq. 9 (- - - -) for $\Delta \approx 0.4\delta_{th}$ (1st column), $1.6\delta_{th}$ (2nd column) and $2.8\delta_{th}$ (3rd column) in cases A-E (1st -5th row). All the terms are normalised with respect to $\rho_0 S_L^2 / \delta_{th}^2$.

Figure 5: Variations of T_3 (—) and $(T_3)_{res}$ (—●—) conditionally averaged in bins of \tilde{c} along with the predictions of eqs.12i and 12iii (—×—) and eqs. 13i and 13ii (- - - -) for $\Delta \approx 0.4\delta_{th}$ (1st column), $\Delta \approx 1.6\delta_{th}$ (2nd column) and $\Delta \approx 2.8\delta_{th}$ (3rd column) in cases A-E (1st -5th row). All the terms are normalised with respect to $\rho_0 S_L^2 / \delta_{th}^2$.

Figure 6: Variations of $[T_4 + f(D) - D_2]$ (—) and $[(T_4)_{sg} - (D_2)_{sg} + \{f(D)\}_{sg}]$ (—●—) conditionally averaged in bins of \tilde{c} along with the predictions of eqs.15i and 15ii (—×—) and eq. 16 (- - - -) for $\Delta \approx 0.4\delta_{th}$ (1st column), $1.6\delta_{th}$ (2nd column) and $2.8\delta_{th}$ (3rd column) in cases A-E (1st -5th row). All the terms are normalised with respect to $\rho_0 S_L^2 / \delta_{th}^2$.

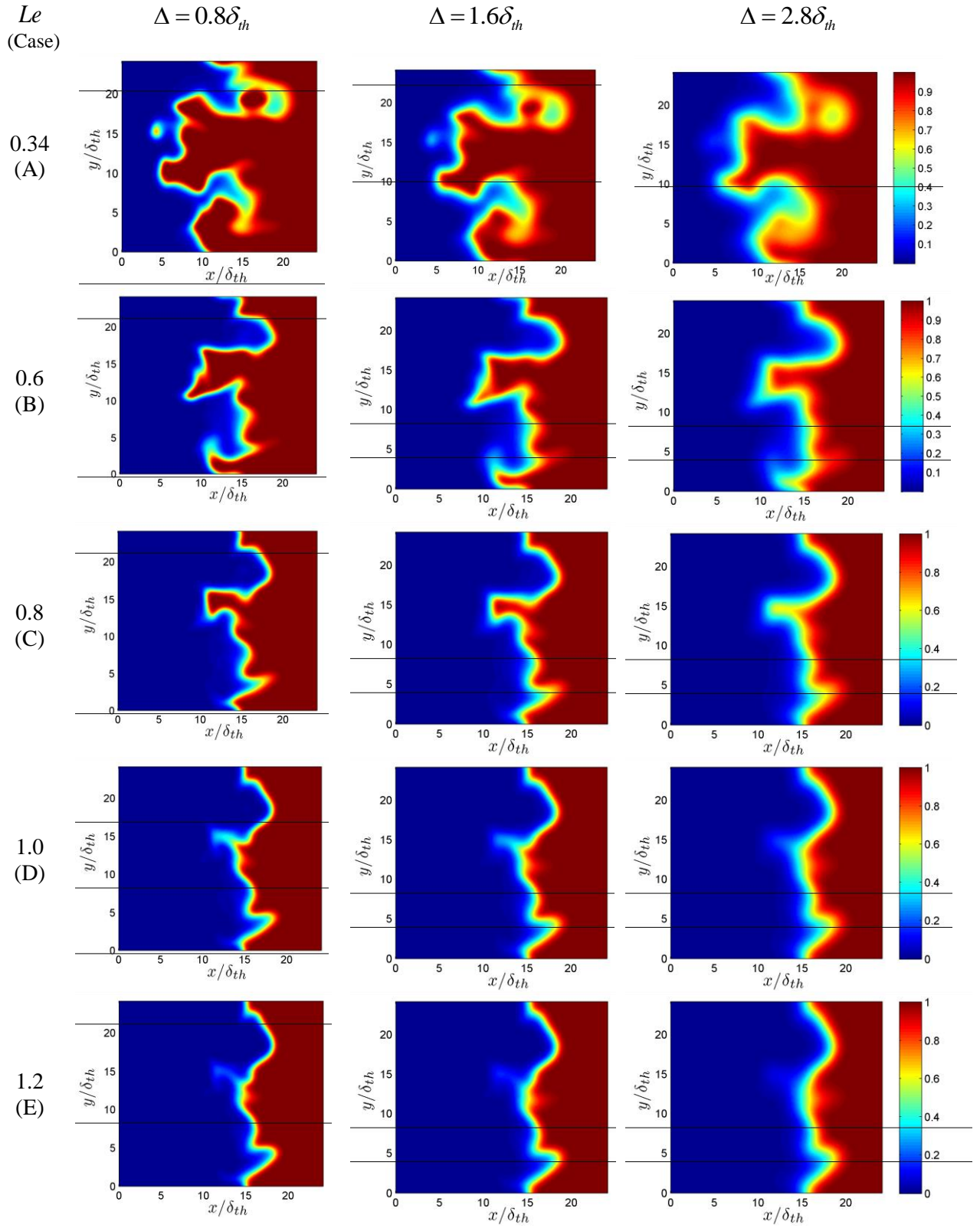


Figure 1: Distributions of \tilde{c} on $x_1 - x_2$ mid-plane for $\Delta = 0.8\delta_{th}$ (1st column); $1.6\delta_{th}$ (2nd column); $2.8\delta_{th}$ (3rd column) for cases A-E (1st -5th row) when the statistics were extracted (i.e. $t = 1.75\alpha_{T0}/S_L^2$).

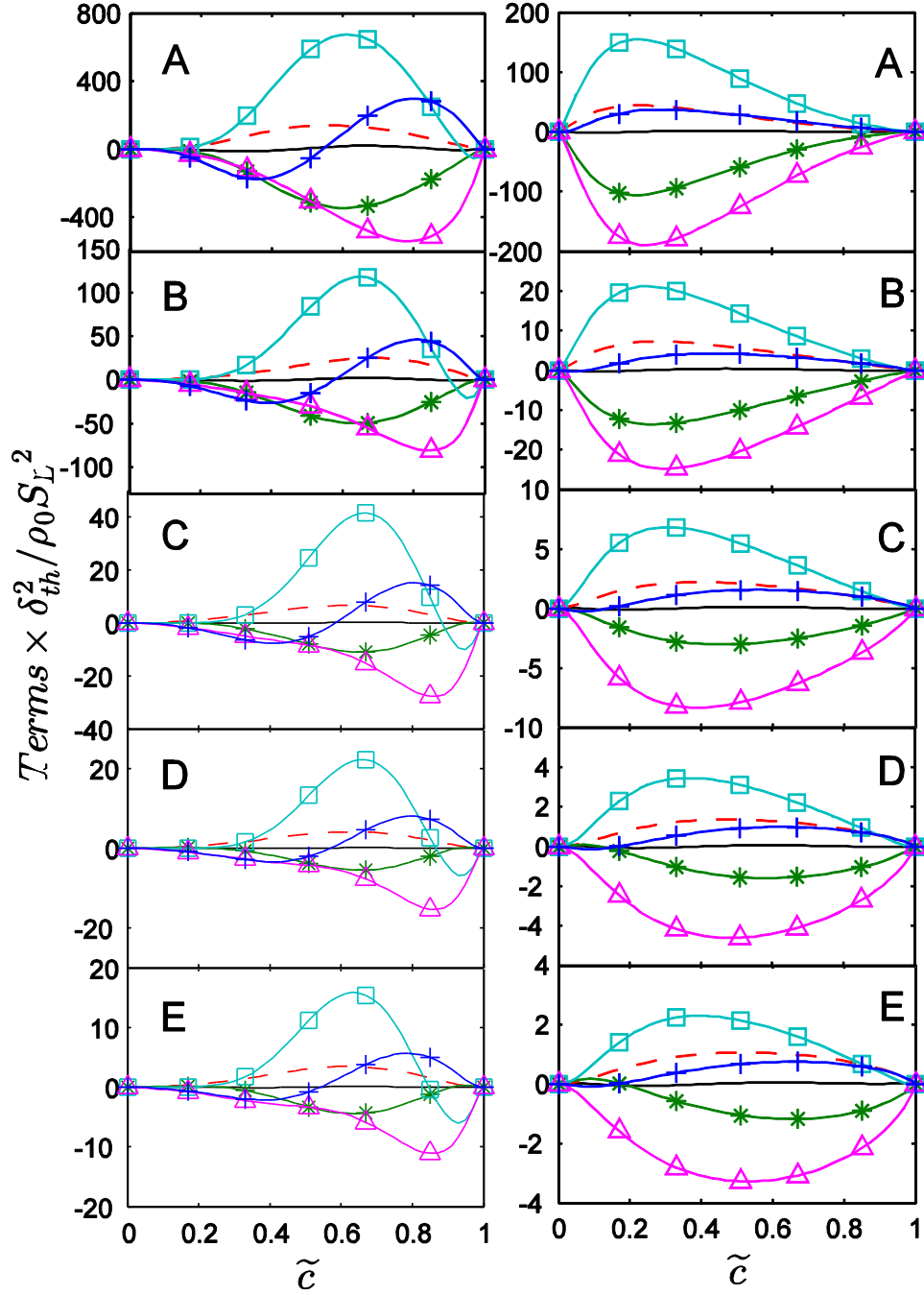


Figure 2: Variations of T_1 (—), T_2 (---), T_3 (—*), T_4 (—□—), $(-D_2)$ (—△—) and $f(D)$ (—+—) conditionally averaged in bins of \tilde{c} for $\Delta \approx 0.4\delta_{th}$ (1st column), $1.6\delta_{th}$ (2nd column) and $2.8\delta_{th}$ (3rd column) in cases A-E (1st-5th row). All the terms are normalised with respect to $\rho_0 S_L^2 / \delta_{th}^2$.

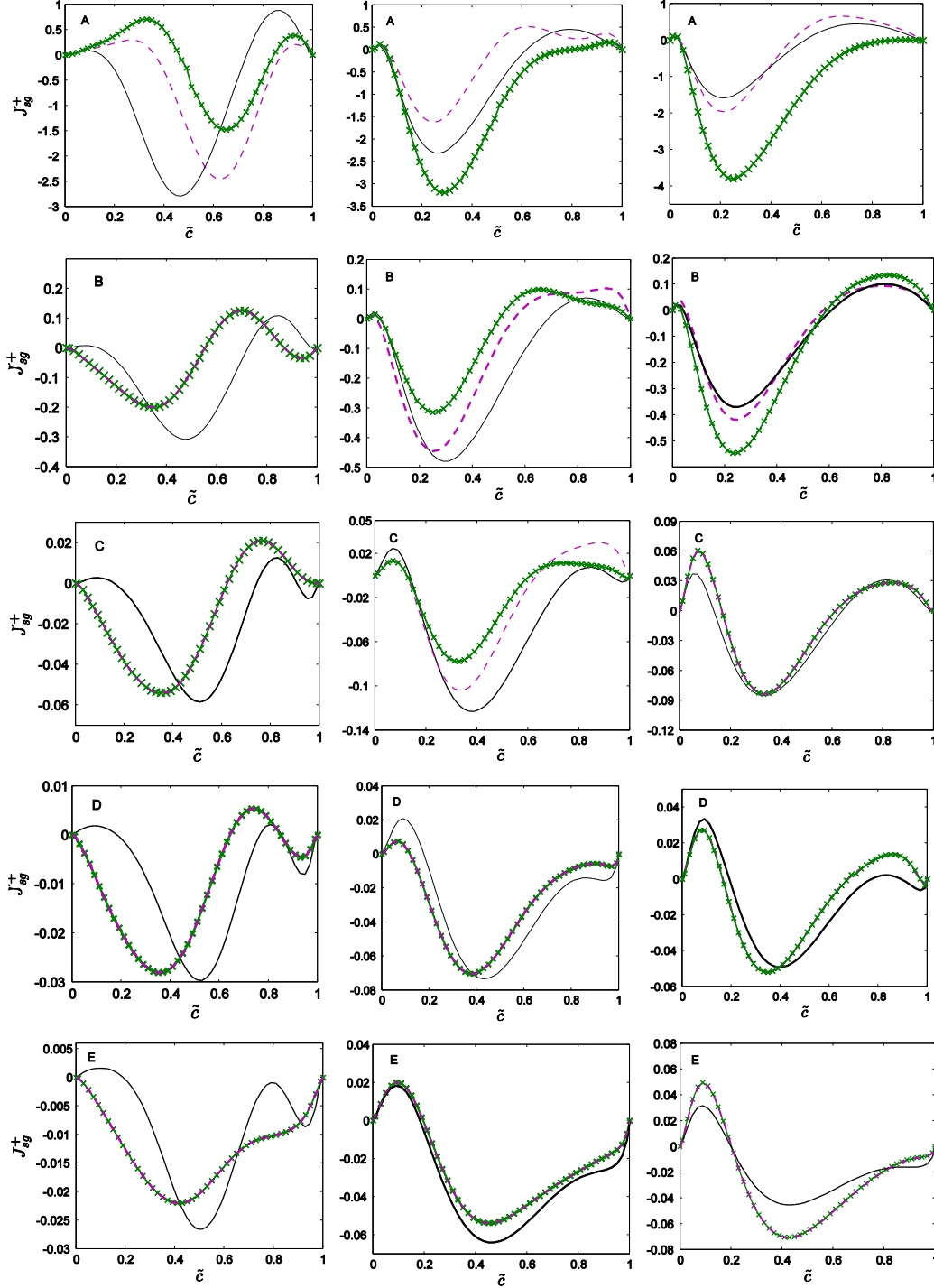


Figure 3: Variations of $J_{sg}^+ = \overline{(\rho u_i N_c - \tilde{\rho} \tilde{u}_i \tilde{N}_c)} M_i \times \delta_{th} / \rho_0 S_L^2$ (—) conditionally averaged in bins of \tilde{c} along with the predictions of eqs. 6i and 6ii with $\Phi' = 0.7$ ($\text{---}\times\text{---}$) and eq. 6i and 6ii with Φ' according to eq. 6iii ($\text{---}\text{---}$) for $\Delta \approx 0.4\delta_{th}$ (1st column), $1.6\delta_{th}$ (2nd column) and $2.8\delta_{th}$ (3rd column) in cases A-E (1st-5th row).

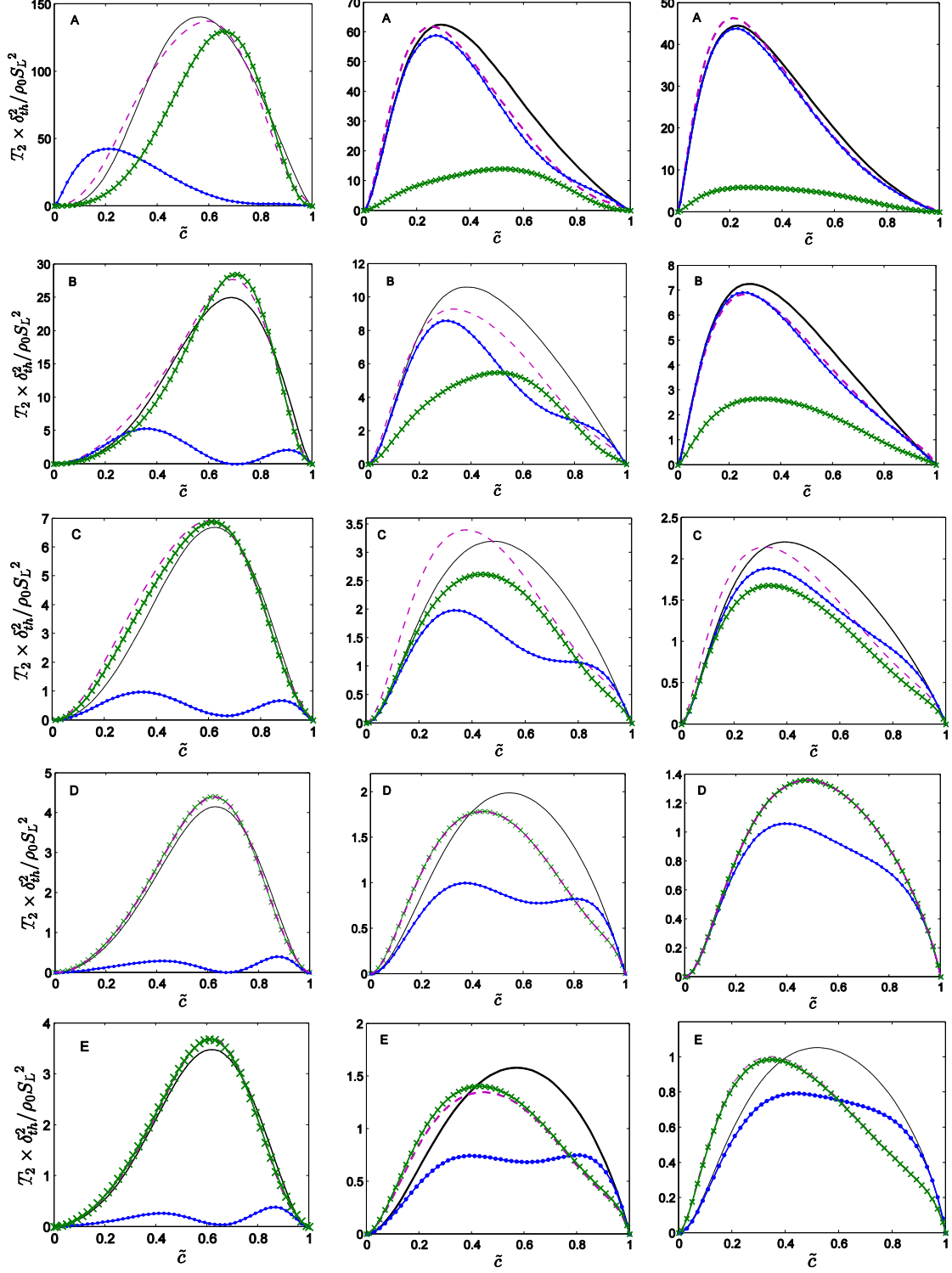


Figure 4: Variations of T_2 (—) and $(T_2)_{sg}$ (—●—) conditionally averaged in bins of \tilde{c} along with the predictions of eq.8 (—×—) and eq. 9 (—◆—) for $\Delta \approx 0.4\delta_{th}$ (1st column), $1.6\delta_{th}$ (2nd column) and $2.8\delta_{th}$ (3rd column) in cases A-E (1st-5th row). All the terms are normalised with respect to $\rho_0 S_L^2 / \delta_{th}^2$.

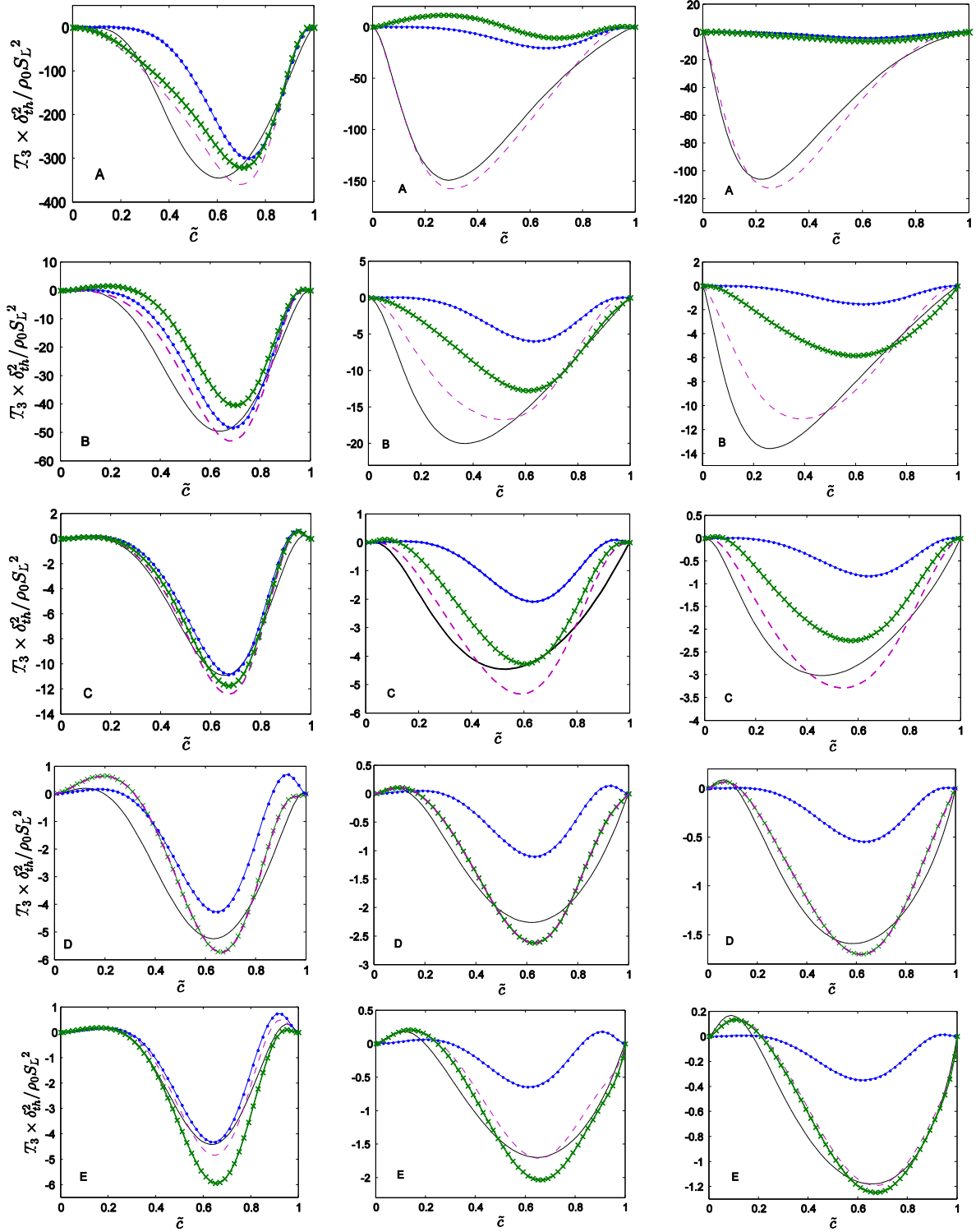


Figure 5: Variations of T_3 (—) and $(T_3)_{res}$ (—●—) conditionally averaged in bins of \tilde{c} along with the predictions of eqs.12i and 12iii (—×—) and eqs. 13i and 13ii (— — —) for $\Delta \approx 0.4\delta_{th}$ (1st column), $\Delta \approx 1.6\delta_{th}$ (2nd column) and $\Delta \approx 2.8\delta_{th}$ (3rd column) in cases A-E (1st-5th row). All the terms are normalised with respect to $\rho_0 S_L^2 / \delta_{th}^2$.

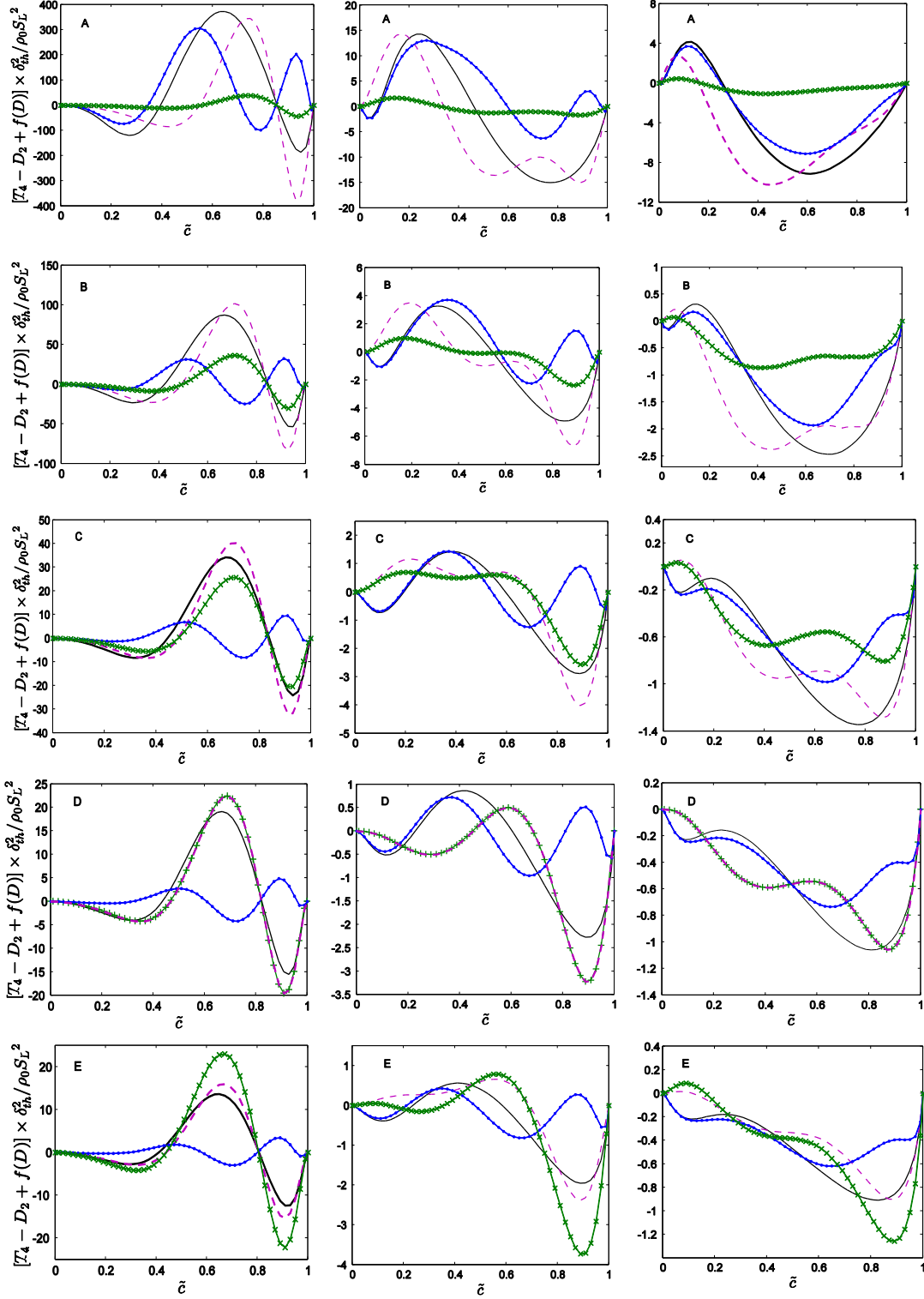


Figure 6: Variations of $[T_4 + f(D) - D_2]$ (—) and $[(T_4)_{sg} - (D_2)_{sg} + \{f(D)\}_{sg}]$ (—●—) conditionally averaged in bins of \tilde{c} along with the predictions of eqs.15i and 15ii (—×—) and eq. 16 (---) for $\Delta \approx 0.4\delta_{th}$ (1st column), $1.6\delta_{th}$ (2nd column) and $2.8\delta_{th}$ (3rd column) in cases A-E (1st-5th row). All the terms are normalised with respect to $\rho_0 S_L^2 / \delta_{th}^2$.